

Tunable Optoelectronic Properties of Triply-Bonded Carbon Molecules with Linear and Graphyne Substructures

Deepak Kumar Rai,[†] Himanshu Chakraborty,^{†,‡} and Alok Shukla^{*,†,¶}

[†]*Department of Physics, Indian Institute of Technology Bombay, Powai, Mumbai-400076,
INDIA.*

[‡]*Present Address: Department of Chemistry, Temple University, SERC 701E, 1925 N.
12th Street, Philadelphia, PA 19122, USA*

[¶]*Present Address: Department of Physics, School of Engineering and Applied Sciences,
Bennett University, Plot No 8-11, TechZone II, Greater Noida 201310 Uttar Pradesh,
INDIA*

E-mail: shukla@phy.iitb.ac.in

Abstract

In this paper we present a detailed computational study of the electronic structure and optical properties of triply-bonded hydrocarbons with linear, and graphyne substructures, with the aim of identifying their potential in opto-electronic device applications. For the purpose, we employed a correlated electron methodology based upon the Pariser-Parr-Pople model Hamiltonian, coupled with the configuration interaction (CI) approach, and studied structures containing up to 42 carbon atoms. Our calculations, based upon large-scale CI expansions, reveal that the linear structures have intense optical absorption at the HOMO-LUMO gap, while the graphyne ones have those at higher energies. Thus, the opto-electronic properties depend on the topology of the graphyne substructures, suggesting that they can be tuned by means of structural modifications. Our results are in very good agreement with the available experimental data.

Introduction

Carbon is one of the most important chemical elements on earth, in particular, given its role in the living matter. It is known to exist in various allotropic forms such as fullerenes, nanotubes, graphite, and diamond. Of these, diamond and graphite have been known for a long time, and have widespread industrial applications. Recently, its two-dimensional allotrope graphene was synthesized,¹ which has revolutionized the research in the field of carbon chemistry and physics. But, graphene suffers from the drawback of not having a band gap, which severely limits its potential as far as device applications are concerned. Therefore, the search for a gapped 2D carbon allotrope continues².

In 1987, Baughman, Eckhardt, and Kertesz, based upon the first-principles theory, predicted a layered allotrope of carbon, in which the individual layers consist of hexagonal rings connected to each other by acetylenic linkages ($-C \equiv C-$), and christened it graphyne.³ They found that graphyne has similar mechanical properties, and high-temperature stability, as

graphite, with its interlayer binding energy per carbon atom being -1.07 kcal/mol, compared to -1.36 kcal/mol for graphite. But, unlike graphite, they predicted graphyne to be a direct band gap semiconductor, with a gap of 1.2 eV.³ Other authors who studied graphyne also concluded that it is a stable allotrope of carbon,^{4,5} which has the potential for device applications because of its direct band gap.

Based upon the interlayer binding energy of graphyne, one can conclude that if 3D graphyne is synthesized, it will be possible to obtain its monolayer in a way similar to how graphene is derived from graphite. Graphyne monolayers have also been studied theoretically,^{6,7} and predicted to be stable, with a direct band gap ≈ 0.96 eV.⁷ Nanoribbons of graphyne and related structures have also been studied at various levels of theory.⁸⁻¹² Ground state properties of finite hydrogen-passivated graphyne substructures were investigated using the first principles theory by Tahara et al.¹³ Several groups have synthesized hydrocarbon analogs of finite graphyne-like structures, and measured their optical absorption spectra.^{5,14,15} Haley and co-workers⁵ measured the UV-vis spectra of various graphyne substructures highlighting the strong structure-property relationship. The present work aims to understand the relationship between the topologies of these structures, and their optical properties, by theoretical means. Such an understanding can facilitate the development of novel graphyne based opto-electronic devices. To the best of our knowledge no theoretical studies of their excited states, and optical properties have been performed as yet. Structures studied in this work are shown in Fig. 1, and can be grouped in two classes: (a) linear units, and (b) graphyne units. Because the unit cell of a graphyne monolayer consists of a triangular structure with hexagonal rings at the vertices, connected to each other by acetylenic linkages, we refer to all fragments with this unit as graphyne substructures. The common point between these two types of structures is the presence of acetylenic linkages.

Theoretical Methodology

Symmetry Considerations

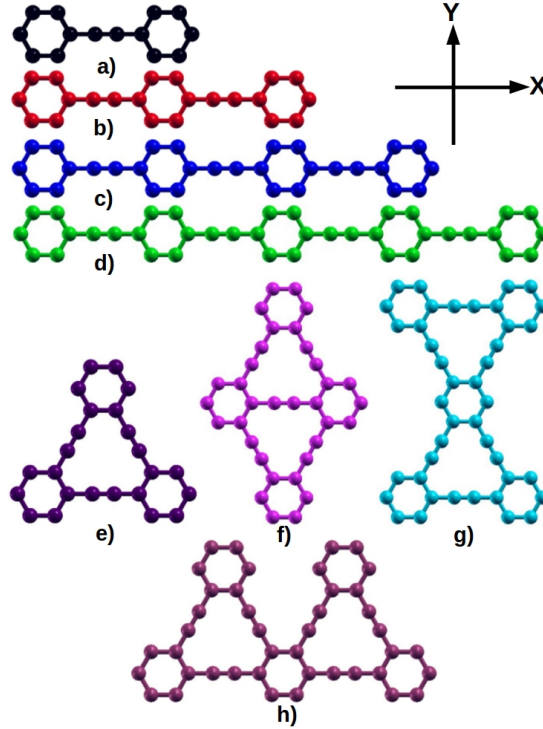


Figure 1: Schematic diagrams of molecules with linear (a)–(d), and graphyne substructures (e)–(h), where dots denote the carbon atoms.

The molecules considered in this work (see Fig. 1) belong to two classes: (a) linear units (LUs or LU- n), and (b) graphyne units (GUs or GU- n), where n is the total number of carbon atoms in a given molecule. LUs belong to the point group D_{2h} (Figs. 1a-1d) while GUs belong to a variety of point groups: D_{2h} (Figs. 1f-1g), D_{3h} (Fig. 1e), and C_{2v} (Fig. 1h). Irreducible representations (irreps) of the ground states of molecules with symmetries D_{2h} , D_{3h} , and C_{2v} , are 1A_g , ${}^1A'_1$, and 1A_1 , respectively. Therefore, as per dipole selection rules, irreducible representations of excited state of these structures, accessible through one-photon transitions, will be: (a) ${}^1B_{2u}$ (y -polarized), and ${}^1B_{3u}$ (x -polarized), for D_{2h} molecules, (b) doubly degenerate ${}^1E'$ (xy plane polarized), for D_{3h} molecules, and (c) 1A_1 (y -polarized)

and 1B_2 (x -polarized), for C_{2v} molecules.

PPP Model Hamiltonian

These calculations have been carried out by employing the PPP model Hamiltonian,^{16,17} given by

$$H = -\sum_{i,j,\sigma} t_{ij} \left(c_{i\sigma}^\dagger c_{j\sigma} + c_{j\sigma}^\dagger c_{i\sigma} \right) + U \sum_i n_{i\uparrow} n_{i\downarrow} + \sum_{i<j} V_{ij} (n_i - 1)(n_j - 1) \quad (1)$$

where $c_{i\sigma}^\dagger$ ($c_{i\sigma}$) are creation (annihilation) operators corresponding to a π electron of spin σ , localized on the i -th carbon atom, while the total number of electrons with spin σ on atom i is given by the corresponding number operator $n_i = \sum_\sigma c_{i\sigma}^\dagger c_{i\sigma}$. The second and third terms in Eq. 1 denote the electron-electron repulsion terms, with the parameters U and V_{ij} representing the on-site, and the long-range Coulomb interactions, respectively. The t_{ij} depicts one-electron hopping matrix elements, which, in this work, have been restricted to the nearest neighbors. All our earlier works on π -electron systems such as conjugated polymers,¹⁸ poly-aromatic hydrocarbons,^{19,20} and graphene quantum dots²¹ involved molecules containing only single and double carbon bonds, for which PPP model has been parameterized extensively over the years.²² The common choice of hopping matrix element is $t_0 = 2.4$ eV, corresponding to the C-C bond length of 1.40 Å, while for shorter or longer bonds, its value can be extrapolated using various relationships between the bond length and the hopping, such as the exponential formula used by us earlier.^{23,24} A limiting case of the exponential formula is the linear relationship,

$$t_{ij} = t_0 - \alpha(r_{ij} - r_0) \quad (2)$$

where $t_0 = 2.4$ eV, $r_0 = 1.40$ Å, r_{ij} being the distance (in Å) between sites i and j , and α is an adjustable parameter denoting electron-phonon coupling. A popular choice of parameters for the Coulomb interactions is according to the Ohno relationship²⁵

$$V_{ij} = U/\kappa_{i,j}(1 + 0.6117R_{i,j}^2)^{1/2} \quad (3)$$

where $\kappa_{i,j}$ represents the dielectric constant of the system which replicates screening effects, U as described above is the on-site electron-electron repulsion term, and $R_{i,j}$ is the distance (in Å) between the i -th and the j -th carbon atoms. Earlier calculations have been done in our group for phenylene based polymers (i.e. π -conjugated system), using both the “screened parameters”²² with $U = 8.0$ eV, $\kappa_{i,j} = 2.0 (i \neq j)$ and $\kappa_{i,i} = 1.0$, and the “standard parameters” with $U = 11.13$ eV and $\kappa_{i,j} = 1.0$. In the next section, we investigate the applicability of these parameters to the case of triple-bonded carbon systems investigated in this work.

Independent of the choice of model parameters, computations are initiated by performing mean field restricted Hartree-Fock (RHF) calculations within the PPP model using a code developed in our group, which also transforms the Hamiltonian from the site representation to the molecular-orbital (MO) representation.²⁶ This is followed by correlated calculations at the full configuration interaction (FCI), quadruple configuration interaction (QCI), or at the multi-reference singles-doubles configuration interaction (MRSDCI) level, depending upon the size of the graphyne substructures. In the FCI approach, all possible excitations from HF ground state are considered, while up to quadruple excitations are considered in the QCI approach. Thus, both the FCI and QCI approaches require a significant amount of computational resources and can be performed only for small systems. In MRSDCI calculations, singly and doubly excited configurations from the chosen set of reference configurations of the selected symmetry subspace are considered for generating the CI matrix.^{27,28} Therefore, this approach allows one to perform calculations on larger molecules.^{18,20,21} In this work we have performed FCI calculations on LU-14, QCI for LU-22 and GU-24, while for larger molecules, MRSDCI approach has been employed. For all the CI approaches, point-group and spin symmetries were fully utilized, thus making the calculations efficient. Subsequently these CI wave functions are used to compute transition electric dipole matrix elements between

various states, allowing us to calculate the linear optical absorption cross-section $\sigma(\omega)$,^{18,20,21} using the formula

$$\sigma(\omega) = 4\pi\alpha \sum_i \frac{\omega_{i0} |\langle i | \hat{\mathbf{e}} \cdot \mathbf{r} | 0 \rangle|^2 \gamma}{(\omega_{i0} - \omega)^2 + \gamma^2}, \quad (4)$$

where ω is the frequency of the incident radiation, $\hat{\mathbf{e}}$ denotes its polarization direction, \mathbf{r} is the position operator, α is the fine structure constant, 0 and i , respectively, denote the ground and the excited states, ω_{i0} is the frequency difference between those states, and γ is the absorption line-width. We note that in Eq. 4 summation over all the dipole-allowed excited states is performed, and a Lorentzian line shape is assumed.

Parameterization of PPP model for Triple-Bonded Molecules

Given the fact that this is our first application of the PPP model to triple-bonded π -conjugated molecules, we first investigate its applicability to the simplest molecule studied in this work, LU-14, whose hydrogen-passivated chemical analog is diphenylacetylene. To do so, we first survey the values of various carbon-carbon bond lengths reported by different authors for diphenylacetylene. Similar to the case of graphyne, diphenylacetylene, and all the other molecules considered here have three types of C-C bond lengths corresponding to the phenyl ring, the single bond, and the triple bond. Narita *et al.*⁴ obtained their optimized values for 2D graphyne to be 1.419 Å, 1.401 Å, and 1.221 Å, respectively. Robertson and Woodward,²⁹ based upon X-ray measurements reported identical values of the single and the phenyl ring bond lengths to be 1.40 Å, and triple bond length 1.19 Å, in the crystalline phase of diphenylacetylene. Rosseto *et al.*³⁰ reported spectroscopic measurements on diphenylacetylene, along with PM3/CI level optimized geometries for the gas phase. Their optimized values of the single and the phenyl ring bond lengths were in the range 1.389—1.415 Å, while that of the triple bond was 1.195 Å. Chernia *et al.*³¹ also performed geometry optimization for diphenylacetylene at the PM3/RHF level, and reported 1.195 Å for the triple

bond length, while the other ones were in the range 1.390–1.415 Å. In our earlier works, we showed that the optical absorption spectra computed using the PPP model are insensitive to small changes in the bond lengths.^{23,24} Therefore, to simplify calculations, we considered only two distinct bond lengths: 1.40 Å (phenyl ring and single bond), and 1.22 Å (triple bond), which are close to the optimized bond lengths of 2D graphyne,⁴ and used them in all the molecules including diphenylacetylene. The hopping matrix elements corresponding to these bond lengths were computed using Eq. 2, with $\alpha = 3.4 \text{ eV}/\text{Å}$,³² leading to values 2.4 eV, and 3.012 eV, respectively.

With these hopping matrix elements and bond lengths, we perform PPP-FCI calculations on diphenylacetylene to compute the excitation energy of its first dipole-allowed state 1^1B_{3u} , whose value has been measured to be 4.17 eV by Suzuki.¹⁴ The screened parameters²² ($U = 8.0 \text{ eV}$, $\kappa_{i,j} = 2.0 (i \neq j)$ and $\kappa_{i,i} = 1.0$) based calculations predict 4.49 eV for the excitation energy, while the standard parameters ($U = 11.13 \text{ eV}$ and $\kappa_{i,j} = 1.0$) yield the value 4.52 eV for the same. Thus, calculations based upon both these parameter sets overestimate the excitation energy of 1^1B_{3u} by about 0.3 eV. In order to determine a new set of parameters for the PPP model, for which the FCI value of $E(1^1B_{3u})$ will match perfectly with the experiments, we performed a number of PPP-FCI calculations in which the values of the hopping matrix element corresponding to the triple bond (t_T), and on-site repulsion U were varied, keeping all other parameters and the bond lengths fixed, and the results are presented in Fig. 2. From Fig. 2a it obvious that for $E(1^1B_{3u})$ to be close to the experimental value, hopping t_T has to assume values smaller than 2.5 eV, which is unrealistically small for a triple bond. However, when we reduce U instead, keeping $t_T = 3.012 \text{ eV}$ fixed (see Fig. 2b), we obtain both for (a) standard parameters with $U = 8.92 \text{ eV}$ and $\kappa_{i,j} = 1.0$, and (b) screened parameters $U = 7.117 \text{ eV}$, $\kappa_{i,j} = 2.0 (i \neq j)$ and $\kappa_{i,i} = 1.0$, $E(1^1B_{3u}) = 4.15 \text{ eV}$, which is in excellent agreement with the experimentally observed value of 4.17 eV. Therefore, we adopt these reduced values of U to perform the standard and screened parameter based PPP-CI calculations on all LUs and GUs considered in this work.

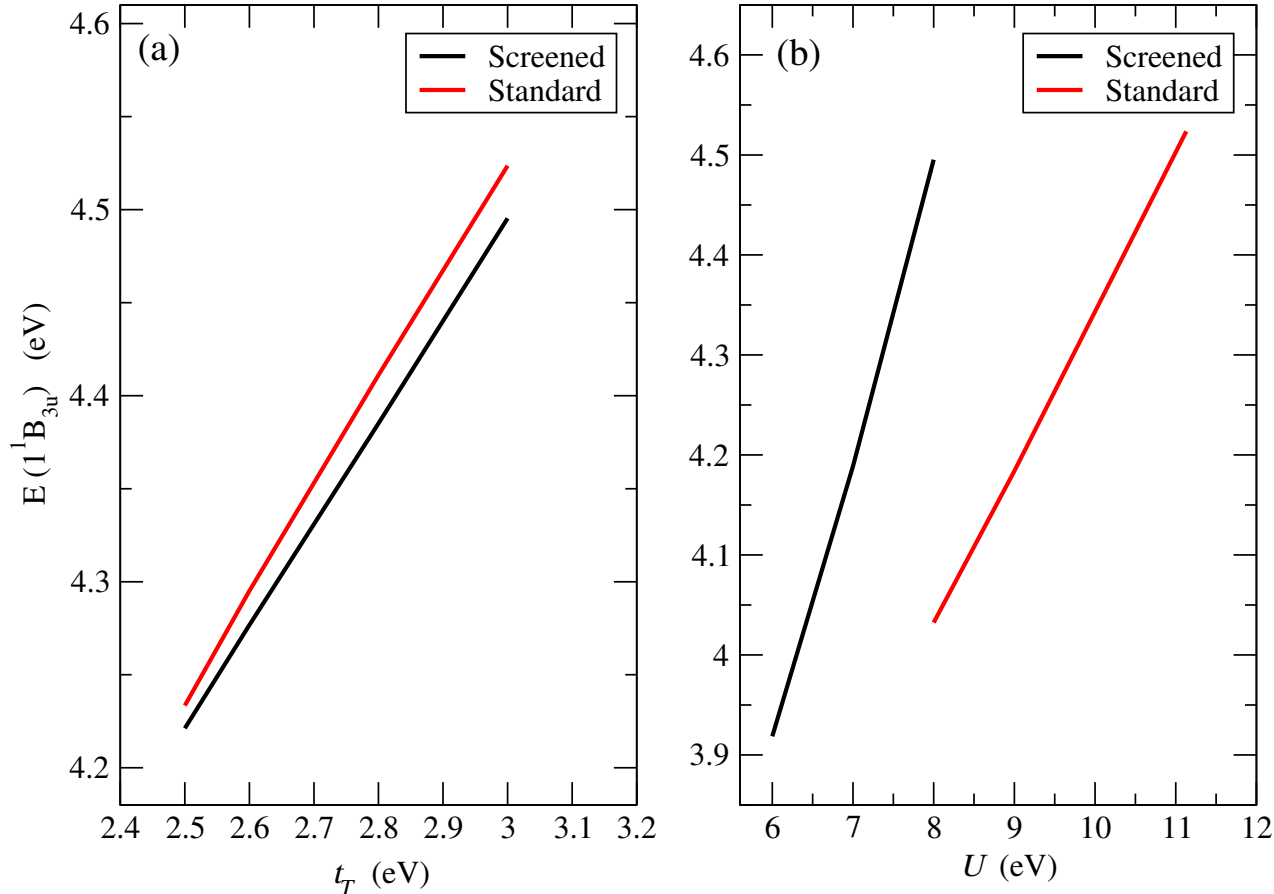


Figure 2: PPP-FCI values of the excitation energy of the 1^1B_{3u} state ($E(1^1B_{3u})$) of diphenylacetylene as a function of: (a) hopping matrix element of the triple bond (t_T), keeping normal values of Coulomb parameters, and (b) on-site repulsion U , keeping normal value of $t_T = 3.012$ eV. Calculations were performed both for standard and screened type Coulomb parameters, keeping bond lengths, and other hopping matrix elements unchanged.

Results and Discussion

Next, we present the calculated optical absorption spectra first for linear molecules, followed by graphyne units. To elucidate the large-scale nature of these calculations, in Table 1 we present the dimensions of the CI matrices employed in these calculations, for various symmetry subspaces, of different molecules. The level of the CI calculation (FCI/QCI/MRDCI), PPP Coulomb parameters employed, and the point group symmetry of the concerned molecule, is also indicated in the table. The large size of the CI expansions suggests that the electron

correlation effects are included accurately in these calculations.

Table 1: Dimension of CI matrix (N_{total}) employed in FCI, QCI, and MRSDCI calculations for different symmetry subspaces of the molecules studied in this work. Superscript a implies use of FCI method, superscript b implies use of QCI method both with the standard and the screened parameters, superscript c implies MRSDI method was used with the screened parameters, superscript d implies MRSDCI method was used with the standard parameters, and superscript e implies that the QCI method was used, without employing the point-group symmetry.

Molecule	Point Group	Total Number of configurations (N_{total}) for different symmetries		
LU-14	D_{2h}	$626264^a (^1A_g)$	$618240^a (^1B_{2u})$	$621166^a (^1B_{3u})$
LU-22	D_{2h}	$1004267^b (^1A_g)$	$1705926^b (^1B_{2u})$	$1708391^b (^1B_{3u})$
LU-30	D_{2h}	$169177^c (^1A_g)$	$1625960^c (^1B_{2u})$	$837492^c (^1B_{3u})$
		$83634^d (^1A_g)$	$2463474^d (^1B_{2u})$	$590078^d (^1B_{3u})$
LU-38	D_{2h}	$389591^c (^1A_g)$	$2462148^c (^1B_{2u})$	$3214650^c (^1B_{3u})$
		$120957^d (^1A_g)$	$2776450^d (^1B_{2u})$	$1470530^d (^1B_{3u})$
GU-24	D_{3h}	$8176875^e (^1A'_1)$	$8176875^e (^1E')$	—
GU-34	D_{2h}	$315275^c (^1A_g)$	$3506568^c (^1B_{2u})$	$4059445^c (^1B_{3u})$
		$359758^d (^1A_g)$	$3020306^d (^1B_{2u})$	$2849252^d (^1B_{3u})$
GU-42	D_{2h}	$2315782^c (^1A_g)$	$5720562^c (^1B_{2u})$	$4122852^c (^1B_{3u})$
		$3118837^d (^1A_g)$	$7076570^d (^1B_{2u})$	$5894354^d (^1B_{3u})$
GU-42	C_{2v}	$3545794^c (^1A_1)$	$4921592^c (^1B_2)$	—
		$4022004^d (^1A_1)$	$3722918^d (^1B_2)$	—

^aFCI method with the standard and the screened parameters. ^bQCI method with the standard and the screened parameters. ^cMRSDCI method with the screened parameters. ^dMRSDCI method with the standard parameters. ^eQCI method without using the point group symmetry.

Absorption Spectra of Linear Molecules

The calculated optical absorption spectra of LUs using the screened and the standard Coulomb parameters in the PPP model are presented in Figs. 3 (a)–(d), and 4 (a)–(d), respectively. Detailed information about the excited states contributing to various peaks in the computed spectra, including their many-particle wave functions, are presented in Tables S1 to S11 of Supporting Information. A careful examination of the spectra reveals the following trends: (a) with the increasing size of the LUs, the absorption spectra get red shifted, (b) the first peak of the absorption spectra of various molecules, which is mainly due to the

$HOMO (H) \rightarrow LUMO (L)$ excitation, is the most intense one, and always x -polarized, (c) the location of the first peak exhibits weak dependence on the PPP Coulomb parameters, however, higher energy peaks do depend significantly on their values, and (d) the wave functions of most of the states contributing to the absorption spectra are dominated by single excitations, except for a few peaks.

Table 2: Comparison of computed peak locations in the spectra of LU-14, LU-22, and LU-38, with the experimental values; all energies are in eV. For LU-38, F/S in the parentheses implies film/solution based results. Columns with headings Scr/Std contain results of calculations performed using the screened/standard parameters in the PPP model.

System	Experimental values	This Work	
		Scr	Std
LU-14	4.17 (Ref. ¹⁴)	4.15 (¹ B_{3u})	4.15 (¹ B_{3u})
	5.22 (Ref. ¹⁴)	5.23 (¹ B_{2u})	5.65 (¹ B_{3u})
	6.30 (Ref. ¹⁴)	6.35 (¹ $B_{3u}/^1B_{2u}$)	5.81 (¹ B_{2u})
LU-22	3.85 (Ref. ³³), 3.87(Refs. ³⁴⁻³⁶), 3.78(Ref. ³⁷)	3.85 (¹ B_{3u})	3.72 (¹ B_{3u})
	5.32 (Ref. ³⁷), 5.39(Ref. ³⁵)	5.28 (¹ B_{2u})	5.18 (¹ B_{3u})
LU-38	3.07 (F), 3.26(S) (Ref. ³⁸)	3.04 (¹ B_{3u})	3.26 (¹ B_{3u})
	3.77 (F), 3.52 (S) (Ref. ³⁸)	3.98 (¹ B_{3u})	-
	5.06 (F), 4.44 (S) (Ref. ³⁸)	5.00 (¹ B_{3u})	4.28 (¹ B_{3u})

A comparison of the calculated peak positions with the experimental measurements for LU-14, LU-22, and LU-38 is presented in Table 2, while for LU-30, we could not locate any experimental data. Dale,³⁹ Suzuki,¹⁴ and Rosseto et al.³⁰ reported the measurements of the optical absorption in diphenylacetylene (chemical analog of LU-14), which are in good agreement with each other. In particular, Suzuki¹⁴ classified the absorption in three bands labeled A, B, and C, located at 4.17 eV, 5.22 eV, and 6.30 eV, respectively. If, in our spectrum calculated using the screened parameters (*see* Fig. 3), we identify peak I with A band, peak II with B band, and the middle of peaks III and IV as the C band, we obtain excellent agreement with the experiments, as is obvious from that table. Standard parameter based

calculations, on the other hand, are in poor agreement with the experimental locations of bands B and C. As far as intensity profiles are concerned, we do have a slight disagreement with the experimental data in that the measured intensity of C band is somewhat higher than that of the A band, while computed value is somewhat lower. However, both the theory and the experiment agree regarding the relative intensity of the B band. Excellent quantitative agreement between our screened parameter based results and experimental peak locations for this system gives us confidence that our PPP-CI methodology, and the new set of Coulomb parameters, are applicable to triple bonded carbon systems.

Several groups have reported the measurement of the absorption spectrum of 1,4-Bis (phenylethynyl)benzene, the structural analog of LU-22,³⁴⁻³⁷ and report two major peaks located near 3.87 eV and 5.32 eV. Our screened parameter values of 3.85 eV and 5.28 eV are in excellent agreement with the experimental values (see Table 2). Of course, our calculations predict several other absorption peaks of LU-22, which can be verified in future experiments on this system.

Fenenko *et al.*³⁸ reported the measurement of an absorption spectrum of the chemical analog of LU-38, namely, 1,4-bis (4-(phenylethynyl) phenylethynyl) benzene, both in the thin film, and the solution phase. We note that their film based measurements covered a broader spectral range, nevertheless, in Table 2 we compare our computed results to both solution and film based measurements. These authors estimated the band gap of the material in film phase to be 3.07 eV,³⁸ which is in excellent agreement with the $H \rightarrow L$ excitation energy of 3.04 eV, obtained using the screened parameters. Further, Fenenko *et al.*³⁸ reported two peaks at 3.25 eV and 3.51 eV for which our computed spectrum has no counterparts. Out of the two, the first one is close to the band gap, and hence could be a part of the corresponding vibrational sub-band. Their higher energy region reports two more peaks at 3.77 eV and 5.06 eV, which are again in good agreement with our two screened parameter calculated peaks at 3.98 eV and 5.00 eV, respectively. Furthermore, the intensity profile of the film-based measured spectrum is in excellent agreement with that computed using the screened

parameters.

In the solution phase, absorption measurement of Fenenko *et al.*³⁸ was restricted to a narrow spectral window centered around the first absorption peak. They report the main absorption peak at 352 nm (3.52 eV), with a subpeak at 279 nm (4.44 eV), and an intense shoulder at 380 nm (3.26 eV). When compared to screened parameter results, measured values look blue-shifted. However, the first measured absorption peak at 3.26 eV, classified as a shoulder by the authors, is in excellent agreement with our standard parameter result also at 3.26 eV (see Table 2). The main absorption peak of the solution phase located at 3.52 eV, which is less intense compared to the measured shoulder at 3.26 eV, is blue-shifted compared to both the screened and the standard parameter based results. Similarly, the measured peak at 4.44 eV, is somewhat blue-shifted compared to the standard parameter based peak computed at 4.28 eV. Thus, we conclude that standard parameter based theory is in better agreement with the solution based results for LU-38, while the screened parameter results are in better agreement with the film based measurements. This, on physical grounds, is quite understandable, because screening effects will be prominent in the film phase. In the solution phase, molecules are isolated, therefore, there will be hardly any screening due to the presence of other molecules.

We also note that the location of the first peak of the LUs considered varies from 3.04 eV to 4.15 eV, which covers visible to near ultraviolet region. Thus, these molecules can be useful for building optoelectronic devices in a fairly broad spectral range.

Absorption Spectra of Graphyne Substructures

Next, we present the results of our calculations of the optical absorption spectra of GUs, performed with the screened and the standard parameters in Figs. 3 (e)–(h), and 4 (e)–(h), respectively. In Tables 3–6, we make a comparison between our calculated peak position in the spectra of various GUs, with the corresponding experimental values, while detailed information about the excited states (energies, transition dipoles, wave functions etc.) is

presented in Tables S12 to S23 of the Supporting Information. A large number of measurements of optical absorption spectra of hydrocarbons, which are structural analogues of GUs, have been reported in the literature.^{3,5,15,40–48}

Hydrocarbon analogue of GU-24 (Fig. 1e) is tribenzo[12]annulene, whose UV-Vis spectrum was first measured by Campbell *et al.*⁴⁴, and later on by several other workers.^{5,40–43,45,47,49} All the reported measurements agree with each other in that absorption spectrum consists of a strongly allowed band near 290 nm (4.26 eV), a weakly allowed band near 350 nm (3.54 eV),⁴⁵ and a strongly forbidden band at 400 nm (3.09 eV).⁴⁵ Our PPP-CI calculations, employing the screened parameters, predict the first, and the most intense, absorption peak at 4.32 eV, which corresponds to a doubly degenerate state of ${}^1E'$ symmetry. The same calculations predict a dipole forbidden state dominated by the singly-excited configuration $|H \rightarrow L\rangle$ at 3.15 eV. We note that as per selection rules of the D_{3h} point group, $H \rightarrow L$ transition is dipole forbidden because it belongs to ${}^1A_2''$ symmetry. Our calculations also predict a doubly degenerate state of ${}^1E'$ symmetry, located at 3.48 eV, which is optically forbidden because it has the same particle-hole symmetry as the ground state. But, the particle-hole symmetry is an approximate symmetry which is an artifact of employing the nearest-neighbor tight-binding model in the calculations, and, therefore, optical transitions forbidden due to it, are in fact weakly allowed in nature. Therefore, our calculated ${}^1E'$ state at 3.48 eV is a strong candidate for weakly allowed state seen in the experiments at 3.54 eV. Thus, the screened parameter results are in very good agreement with the experiments, while it is obvious from Table 3 that our standard parameter based PPP results disagree with the experiments significantly. We note that both the strongly allowed (4.32 eV) and forbidden state (3.48 eV) are dominated by same singly excited configurations, with wave functions containing the configurations $|H \rightarrow (L + 1)_1\rangle \pm c.c.$ and $|H \rightarrow (L + 1)_2\rangle \pm c.c.$ Our calculations also predict several higher energy peaks of weaker intensity, which we hope will be detected in future experiments.

Table 3: Comparison of computed peak locations in the spectra of GU-24 with the experimental values. Rest of the information is same as in the caption of Table 2.

Experimental values	This Work	
	Scr	Std
3.54 (Ref. ⁴⁵),3.59(Ref. ⁴⁰),3.60 (Ref. ⁴²),3.61 (Ref. ⁴³), 3.62 (Ref. ¹⁵),3.62 (Ref. ⁴¹),3.66(Ref. ³),	3.48	3.72
4.20(Ref. ⁵),4.20 (Ref. ⁴²),4.20 (Ref. ⁴¹), 4.20(Ref. ¹⁵),4.24(Ref. ⁴⁰),4.27(Ref. ⁴⁵) 4.28(Ref. ⁴³),4.29(Ref. ⁴⁴),		
4.32(Ref. ⁴⁰),4.33 (Ref. ⁴¹), 4.33 (Ref. ⁴²), 4.33 (Ref. ¹⁵),4.39(Ref. ⁵),	4.32 (^{1E'})	4.38 (^{1E'})
4.45(Ref. ⁴⁰),4.45 (Ref. ⁴¹), 4.45 (Ref. ⁴²), 4.42 (Ref. ⁴⁵),4.45 (Ref. ¹⁵),4.49 (Ref. ⁴⁵), 4.57(Ref. ⁵),		
4.73 (Ref. ⁴²), 4.73 (Ref. ⁴¹),4.80(Ref. ⁴⁰),		
5.06(Ref. ⁴¹)	5.12 (^{1E'})	5.21 (^{1E'})

Table 4: Comparison of computed peak locations in the spectra of GU-34 with the experimental values. MI denotes the peak of maximum intensity. Rest of the information is same as in the caption of Table 2.

Experimental values			This Work	
Ref. ¹⁵	Ref. ⁴⁹	Ref. ⁵	Scr	Std
3.38	3.39	3.44	3.34 (^{1B_{3u}})	2.47 (^{1B_{3u}})
3.54	3.78	3.83	3.51 (^{1B_{2u}})	3.97 (^{1B_{3u}})(MI)
3.71	3.97 (MI)	4.06(MI)	4.18 (^{1B_{3u}})(MI)	4.06 (^{1B_{2u}})(MI)
4.09(MI)	4.09	4.20	4.23 (^{1B_{2u}})(MI)	4.58 (^{1B_{3u}})
4.26	4.24	4.33	—	—
4.38	—	—	—	—

Table 5: Comparison of computed peak locations in the spectra of GU-42 (D_{2h}) with the experimental values. MI denotes the peak of maximum intensity. Rest of the information is same as in the caption of Table 2.

Experimental values			This Work	
Ref. ⁴⁸	Ref. ⁴⁶	Ref. ⁵	Scr	Std
2.55	3.10	3.40	2.43 (${}^1B_{3u}$)	2.53 (${}^1B_{3u}$)
2.73	3.25	4.02(MI)	3.38 (${}^1B_{2u}$)(MI)	3.72 (${}^1B_{2u}$)(MI)
2.81	4.05 (MI)	3.81	3.64 (${}^1B_{3u}$)	4.13 (${}^1B_{3u}$)
3.10	3.60	4.18	3.81 (${}^1B_{3u}$)	4.87 (${}^1B_{3u}$)
3.59(MI)	3.74	4.30	4.55 (${}^1B_{3u}$)	—
3.99	3.88	—	4.81 (${}^1B_{2u}$)	—
4.92	4.18	—	—	—
—	4.30	—	—	—

Table 6: Comparison of computed peak locations in the spectra of GU-42 (C_{2v}) with the experimental values. MI denotes the peak of maximum intensity. Rest of the information is same as in the caption of Table 2.

Experimental values	This Work	
Ref. ⁴⁷	Scr	Std
3.42 (MI)	2.87 (1B_1)	3.53 (1B_1)
3.56	3.74 (${}^1A_1/{}^1B_1$)(MI)	4.10 (1B_1)
3.69	4.17 (1B_1)	4.37 (1A_1)(MI)
4.09	4.34 (1A_1)	4.61 (1B_1)
4.24	4.57(${}^1A_1/{}^1B_1$)	4.94 (1A_1)
4.38	—	—

GU-34 consists of four benzene rings, with D_{2h} symmetry (see Fig. 1f), whose hydrogen saturated version belongs to dehydrobenzoannulene (DBA) class of compounds. Experimental measurements of the optical absorption spectrum for the hydrogen saturated compound were reported by Tahara *et al.*,¹⁵ and for structures saturated by other groups by Sonoda *et al.*,⁴⁹ and Kehoe *et al.*⁵ Our theoretically computed absorption spectrum (see Fig. 3f) is in excellent qualitative agreement with the experiments in that both experiment and theory report weaker absorption at lower energies, followed by a high intensity peak. Experiments predict the location of the maximum intensity peak (see Table 4) in the range 3.97–4.09 eV, to be compared with our calculated values of 4.20 eV (screened parameters) and 4.02 eV

(standard parameters), with contributions from both the B_{2u} and the B_{3u} symmetry states. This gives the impression that the standard parameter values are in better agreement with the experiments, however, a look at Fig. 4 reveals that the standard parameter based intensity profile of the absorption spectrum predicts the first peak as that of maximum intensity, in disagreement with all the experiments. Furthermore, the lower energy peaks located at 3.34 eV and 3.51 predicted by the screened parameter calculations, are in excellent agreement with the measured values of 3.38 eV and 3.54 eV, reported by Tahara¹⁵ *et al.* Our calculations also predict higher energy peaks which are beyond the spectral range probed by the experiments, and perhaps could be checked in future measurements. Tables S14, S15, and S16 of the Supporting Information contain the wave functions and other detailed information about various states contributing to the computed spectra, from which it is obvious that most of the peaks derive their contributions from single excitations, involving orbitals away from the Fermi level. Furthermore, $H \rightarrow L$ excitation makes an insignificant contribution to the maximum intensity peaks.

GU-42- D_{2h} consists five benzene rings, and 42 carbon atoms in all, arranged in D_{2h} symmetry (see Fig. 1g), and its hydrogen saturated version also belongs to the DBA class. Iyoda *et al.*,⁴⁸ Johnson *et al.*,⁴⁶ and Kehoe *et al.*⁵ have reported the measurements of optical absorption spectra this compound, fully, or partially, saturated by hydrogens. However, there is very significant difference among the results of these experiments, as far as peak locations are concerned. For example, measured locations of the maximum intensity peaks are in the range 3.59–4.05 eV^{5,46,48} Furthermore, measured locations of lowest energy peaks also exhibit significant variation in the range 2.55–3.40 eV.^{5,46,48} On comparison of experimental results to our calculations (Table 5), we find best overall agreement with the results of Iyoda *et al.*,⁴⁸ who reported the first weak peak at 2.55 eV, with the maximum intensity peak at 3.59 eV, in fair agreement with our screened parameter values of 2.43 eV, and 3.38 eV, respectively. We note that the corresponding standard parameter values 2.53 eV and 3.72 eV, are in somewhat better agreement with this experiment. Wave function analysis reveals that

the first weak peak is of B_{3u} symmetry, and is dominated by the $H \rightarrow L$ excitation, while the maximum intensity peak is due to an excited state whose wave function is mainly composed of $|H - 2 \rightarrow L\rangle + c.c.$ configurations (See Tables S17—S19 of Supporting Information).

The last graphyne substructure we discuss also has 42 carbon atoms and five benzene rings, but arranged in C_{2v} symmetry (see Fig. 1h). The only reported measurements of the absorption spectrum of this compound are by Tahara *et al.*,⁴⁷ but on a structure in which five edge carbon atoms were saturated by the *t*-butyl group, instead of hydrogens. Maximum intensity was attributed to a band centered around 3.42 eV, while our screened parameter calculations predict the maximum intensity near 3.74 eV, instead (Table 6). Furthermore, our screened parameter calculations also predict a smaller peak, but of significant intensity, at 2.87 eV, which has not been seen in the experiment. As far as other peaks are concerned, we have good agreement between the experiments and screened parameter results on a few others, as is obvious from Table 6. Our calculations predict the first peak to be dominated by $|H \rightarrow L\rangle$ and $|H-1 \rightarrow L+1\rangle$ excitations, while the most intense one by $|H-2 \rightarrow L\rangle + c.c.$ (See Tables S20—S23 of Supporting Information). On comparing the absorption spectra of GU-42- C_{2v} and GU-42- D_{2h} , we note a red shift in the most intense peak for the D_{2h} symmetry, as compared to that for the C_{2v} structure (see Fig. 3 (g)–(h)). Thus, the locations of the strong absorptions can be used to differentiate between the two symmetries of the GU-42.

Summary and Conclusions

To summarize, we presented a computational study the optical absorption spectra of linear and graphyne substructures all of which contain benzene rings connected by acetylenic linkages. The methodology employed included the electron correlation effects, and our results showed good agreement with the experiments, wherever available. Our calculations predict that for the linear structures, the first peak is of maximum intensity, whose energy decreases monotonically with the increasing size. The many-particle nature of this peak corresponds

to HOMO to LUMO excitations for each linear molecule. For graphyne substructures, however, the situation is more complicated, with their topologies having a profound influence on the location of the maximum intensity peaks. Furthermore, the many-particle nature of the excited states contributing to the high intensity peaks of graphyne substructures are very different, when compared to the linear structures. Thus, strong topology dependence of the optical properties of graphyne substructures, suggests the possibility of synthesizing such molecules with custom-made optical properties, by manipulating their structures.

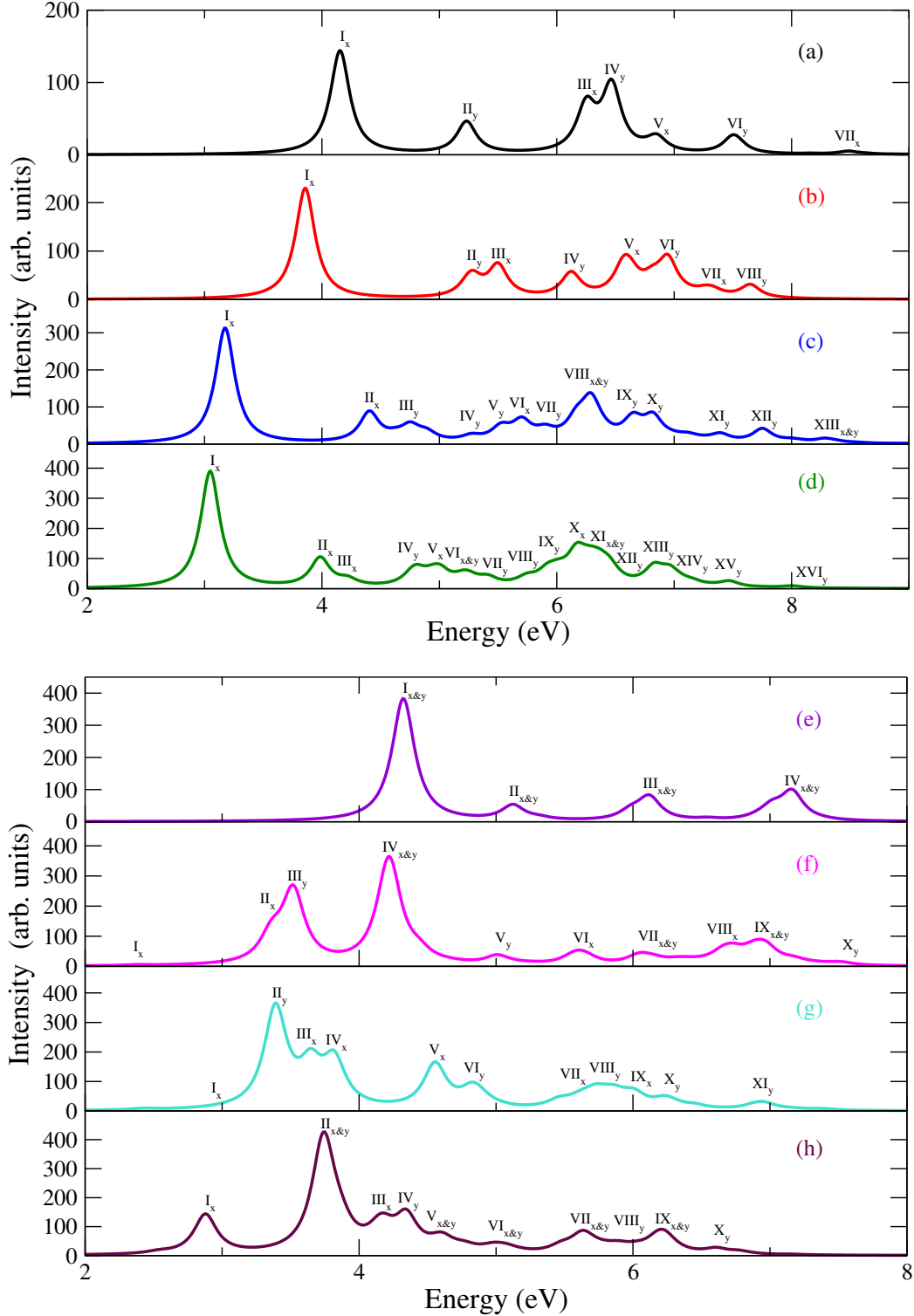


Figure 3: Calculated optical absorption spectra of (a)–(d) triply-bonded linear molecules containing 14–38 atoms, and (e)–(h) graphyne units containing 24–42 carbon atoms, computed using the screened parameters, and the CI approach. The spectra have been broadened with a uniform line-width of 0.1 eV.

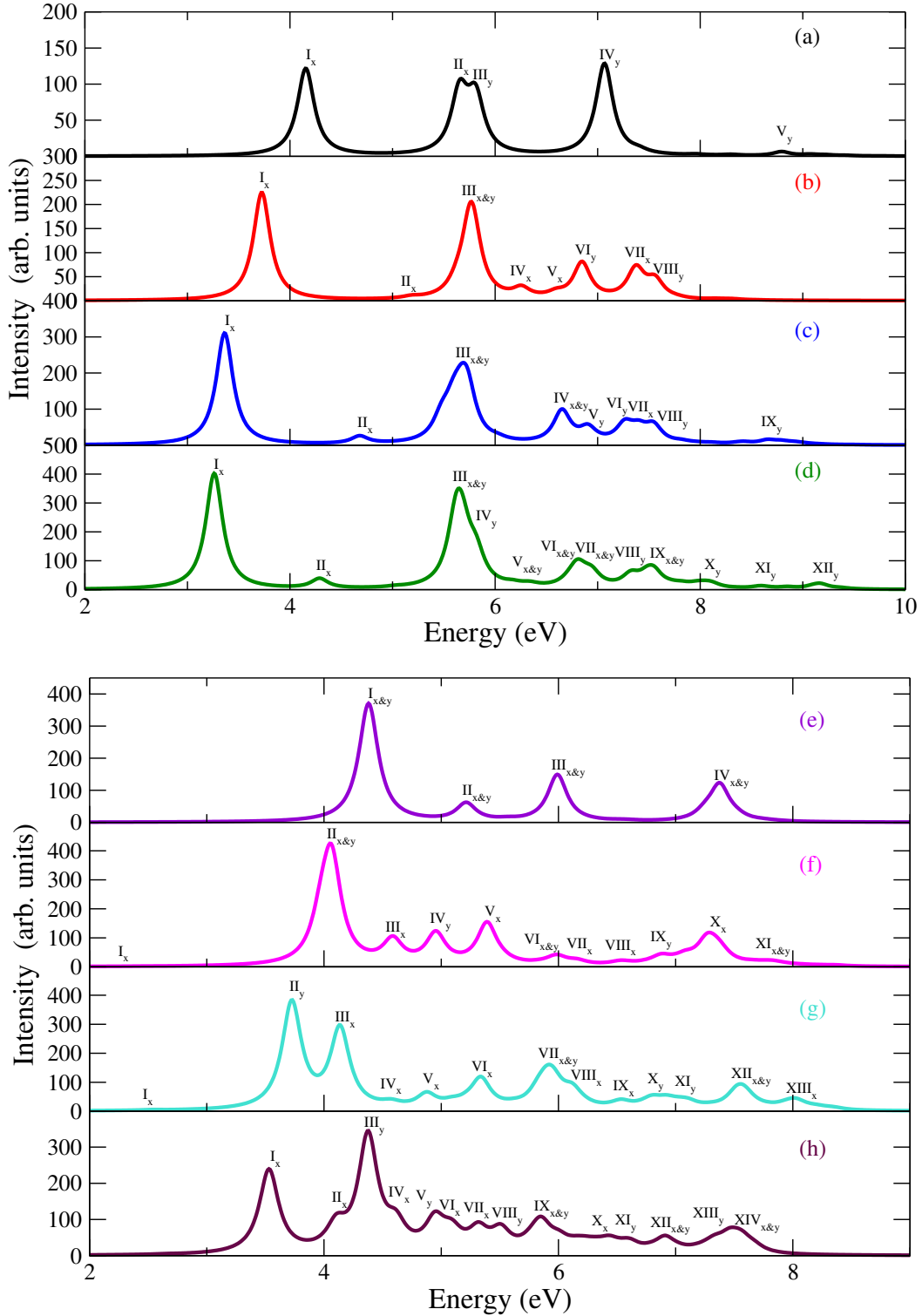


Figure 4: Calculated optical absorption spectra of (a)–(d) linear triply-bonded linear molecules containing 14–38 atoms, and (e)–(h) graphyne substructures containing 24–42 carbon atoms, computed using the standard parameters, and the CI approach. The spectra have been broadened with a uniform line-width of 0.1 eV.

Supporting Information

The Supporting Information is available free of charge on the ACS Publications website at DOI:

Symmetries of various excited states, their excitation energies, dominant terms in their many-body wave-functions and their transition dipole matrix elements with respect to the ground state.

Author Information

Corresponding Authors

Alok Shukla: *E-mail: shukla@phy.iitb.ac.in

Notes

The authors declare no competing financial interests.

Acknowledgements

This research was supported in part by Department of Science and Technology, Government of India, under project no. SB/S2/CMP-066/2013.

References

- (1) Novoselov, K. S.; Geim, A. K.; Morozov, S. V.; Jiang, D.; Zhang, Y.; Dubonos, S. V.; Grigorieva, I. V.; Firsov, A. A. Electric Field Effect in Atomically Thin Carbon Films. *Science* **2004**, *306*, 666–669.
- (2) Peng, Q.; Dearden, A. K.; Crean, J.; Han, L.; Liu, S.; Wen, X.; De, S. New materials

- graphyne, graphdiyne, graphone, and graphane: review of properties, synthesis, and application in nanotechnology. *Nanotechnology, science and applications* **2014**, *7*, 1.
- (3) Baughman, R. H.; Eckhardt, H.; Kertesz, M. Structure-property predictions for new planar forms of carbon: Layered phases containing sp² and sp atoms. *The Journal of Chemical Physics* **1987**, *87*, 6687–6699.
- (4) Narita, N.; Nagai, S.; Suzuki, S.; Nakao, K. Electronic structure of three-dimensional graphyne. *Phys. Rev. B* **2000**, *62*, 11146–11151.
- (5) Kehoe, J. M.; Kiley, J. H.; English, J. J.; Johnson, C. A.; Petersen, R. C.; Haley, M. M. Carbon Networks Based on Dehydrobenzoannulenes. 3. Synthesis of Graphyne Substructures¹. *Organic Letters* **2000**, *2*, 969–972.
- (6) Narita, N.; Nagai, S.; Suzuki, S.; Nakao, K. Optimized geometries and electronic structures of graphyne and its family. *Phys. Rev. B* **1998**, *58*, 11009–11014.
- (7) Kang, J.; Li, J.; Wu, F.; Li, S.-S.; Xia, J.-B. Elastic, Electronic, and Optical Properties of Two-Dimensional Graphyne Sheet. *The Journal of Physical Chemistry C* **2011**, *115*, 20466–20470.
- (8) Pan, L.; Zhang, L.; Song, B.; Du, S.; Gao, H.-J. Graphyne-and graphdiyne-based nanoribbons: density functional theory calculations of electronic structures. *Applied Physics Letters* **2011**, *98*, 173102.
- (9) Yue, Q.; Chang, S.; Kang, J.; Tan, J.; Qin, S.; Li, J. Magnetic and electronic properties of α -graphyne nanoribbons. *The Journal of chemical physics* **2012**, *136*, 244702.
- (10) Wu, W.; Guo, W.; Zeng, X. C. Intrinsic electronic and transport properties of graphyne sheets and nanoribbons. *Nanoscale* **2013**, *5*, 9264–9276.
- (11) Yin, W.-J.; Xie, Y.-E.; Liu, L.-M.; Wang, R.-Z.; Wei, X.-L.; Lau, L.; Zhong, J.-X.;

- Chen, Y.-P. R-graphyne: a new two-dimensional carbon allotrope with versatile Dirac-like point in nanoribbons. *Journal of Materials Chemistry A* **2013**, *1*, 5341–5346.
- (12) Jafari, M.; Asadpour, M.; Majelan, N. A.; Faghinasiri, M. Effect of boron and nitrogen doping on electro-optical properties of armchair and zigzag graphyne nanoribbons. *Computational Materials Science* **2014**, *82*, 391–398.
- (13) Tahara, K.; Yoshimura, T.; Sonoda, M.; Tobe, Y.; Williams, R. V. Theoretical Studies on Graphyne Substructures: Geometry, Aromaticity, and Electronic Properties of the Multiply Fused Dehydrobenzo[12]annulenes. *The Journal of Organic Chemistry* **2007**, *72*, 1437–1442.
- (14) Suzuki, H. Relations between Electronic Absorption Spectra and Spatial Configurations of Conjugated Systems. VI. Triphenylethylene, Tetraphenylethylene and Tolan. *Bulletin of the Chemical Society of Japan* **1960**, *33*, 389–396.
- (15) Tahara, K.; Yamamoto, Y.; Gross, D. E.; Kozuma, H.; Arikuma, Y.; Ohta, K.; Koizumi, Y.; Gao, Y.; Shimizu, Y.; Seki, S. et al. Syntheses and Properties of Graphyne Fragments: Trigonally Expanded Dehydrobenzo[12]annulenes. *Chemistry - A European Journal* **2013**, *19*, 11251–11260.
- (16) Pople, J. A. Electron interaction in unsaturated hydrocarbons. *Trans. Faraday Soc.* **1953**, *49*, 1375–1385.
- (17) Pariser, R.; Parr, R. G. A Semi-Empirical Theory of the Electronic Spectra and Electronic Structure of Complex Unsaturated Molecules. II. *J. Chem. Phys.* **1953**, *21*, 767–776.
- (18) Shukla, A. Correlated theory of triplet photoinduced absorption in phenylene-vinylene chains. *Phys. Rev. B* **2002**, *65*, 125204.

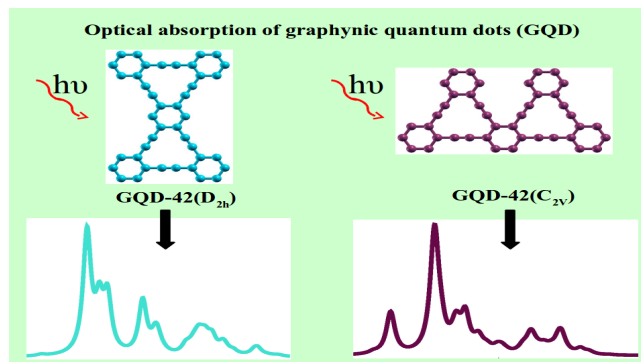
- (19) Aryanpour, K.; Roberts, A.; Sandhu, A.; Rathore, R.; Shukla, A.; Mazumdar, S. Subgap Two-Photon States in Polycyclic Aromatic Hydrocarbons: Evidence for Strong Electron Correlations. *The Journal of Physical Chemistry C* **2014**, *118*, 3331–3339.
- (20) Aryanpour, K.; Shukla, A.; Mazumdar, S. Electron correlations and two-photon states in polycyclic aromatic hydrocarbon molecules: A peculiar role of geometry. *The Journal of Chemical Physics* **2014**, *140*, 104301.
- (21) Basak, T.; Chakraborty, H.; Shukla, A. Theory of linear optical absorption in diamond-shaped graphene quantum dots. *Phys. Rev. B* **2015**, *92*, 205404.
- (22) Chandross, M.; Mazumdar, S. Coulomb interactions and linear, nonlinear, and triplet absorption in poly(para-phenylenevinylene). *Phys. Rev. B* **1997**, *55*, 1497–1504.
- (23) Chakraborty, H.; Shukla, A. Pariser-Parr-Pople Model Based Investigation of Ground and Low-Lying Excited States of Long Acenes. *The Journal of Physical Chemistry A* **2013**, *117*, 14220–14229.
- (24) Chakraborty, H.; Shukla, A. Theory of triplet optical absorption in oligoacenes: From naphthalene to heptacene. *The Journal of Chemical Physics* **2014**, *141*, 164301.
- (25) Ohno, K. Some remarks on the Pariser-Parr-Pople method. *Theoretica chimica acta* **1964**, *2*, 219–227.
- (26) Sony, P.; Shukla, A. A general purpose Fortran 90 electronic structure program for conjugated systems using Pariser-Parr-Pople model. *Computer Physics Communications* **2010**, *181*, 821 – 830.
- (27) Buenker, R.; Peyerimhoff, S. Individualized configuration selection in CI calculations with subsequent energy extrapolation. *Theor. Chim. Acta* **1974**, *35*, 33–58.
- (28) Buenker, R. J.; Peyerimhoff, S. D.; Butscher, W. Applicability of the multi-reference

- double-excitation CI (MRD-CI) method to the calculation of electronic wavefunctions and comparison with related techniques. *Molecular Physics* **1978**, *35*, 771–791.
- (29) Robertson, J.; Woodward, I. X-Ray Analysis of the Dibenzyl Series. V. Tolane and the Triple Bond. *Proc. Royal Soc. (London)* **1938**, *A164*, 436–446.
- (30) Rosseto, R.; Torres, J. C.; Del Nero, J. Modeling of alkynes: synthesis and theoretical properties. *Materials Research* **2003**, *6*, 341–346.
- (31) Chernia, Z.; Livneh, T.; Pri-Bar, I.; Koresh, J. Mode assignment for linear phenyl acetylene sequence: phenylacetylene, di-phenylacetylene and 1,4-di(phenylethynyl)benzene. *Vibrational Spectroscopy* **2001**, *25*, 119 – 131.
- (32) Race, A.; Barford, W.; Bursill, R. J. Low-lying excitations of polydiacetylene. *Phys. Rev. B* **2001**, *64*, 035208.
- (33) Nguyen, P.; Yuan, Z.; Agocs, L.; Lesley, G.; Marder, T. B. Synthesis of symmetric and unsymmetric 1, 4-bis (pR-phenylethynyl) benzenes via palladium/copper catalyzed cross-coupling and comments on the coupling of aryl halides with terminal alkynes. *Inorganica chimica acta* **1994**, *220*, 289–296.
- (34) Levitus, M.; Schmieder, K.; Ricks, H.; Shimizu, K. D.; Bunz, U. H.; Garcia-Garibay, M. A. Steps to demarcate the effects of chromophore aggregation and planarization in poly (phenyleneethynylene) s. 1. Rotationally interrupted conjugation in the excited states of 1, 4-bis (phenylethynyl) benzene. *Journal of the American Chemical Society* **2001**, *123*, 4259–4265.
- (35) Beeby, A.; Findlay, K.; Low, P. J.; Marder, T. B. A re-evaluation of the photophysical properties of 1, 4-bis (phenylethynyl) benzene: A model for poly (phenyleneethynylene). *Journal of the American Chemical Society* **2002**, *124*, 8280–8284.

- (36) Ogoshi, T.; Umeda, K.; Yamagishi, T.-a.; Nakamoto, Y. Through-space [small pi]-delocalized Pillar[5]arene. *Chem. Commun.* **2009**, 4874–4876.
- (37) König, B.; Knieriem, B.; Meijere, A. D. Double-Layered 1, 4-Distyrylbenzene Chromophores–Synthesis, UV and Fluorescence Spectra. *Chemische Berichte* **1993**, *126*, 1643–1650.
- (38) Fenenko, L.; Shao, G.; Orita, A.; Yahiro, M.; Otera, J.; Svechnikov, S.; Adachi, C. Electrical properties of 1, 4-bis (4-(phenylethynyl) phenylethynyl) benzene and its application for organic light emitting diodes. *Chemical Communications* **2007**, 2278–2280.
- (39) Dale, J. Ultraviolet absorption spectra of chain molecules consisting of alternating benzene rings and ethylenic bonds. *Acta Chim. Scand* **1957**, *11*, 971–980.
- (40) Hisaki, I.; Sakamoto, Y.; Shigemitsu, H.; Tohnai, N.; Miyata, M.; Seki, S.; Saeki, A.; Tagawa, S. Superstructure-Dependent Optical and Electrical Properties of an Unusual Face-to-Face, π -Stacked, One-Dimensional Assembly of Dehydrobenzo [12] annulene in the Crystalline State. *Chemistry-A European Journal* **2008**, *14*, 4178–4187.
- (41) Staab, H. A.; Graf, F. Zur Konjugation in makrocyclischen Bindungssystemen, XV. Benzo [12] annulene: 5.6. 11.12. 17.18-Hexadehydro-tribenzo [aei] cyclododecen. *Chemische Berichte* **1970**, *103*, 1107–1118.
- (42) Kamada, K.; Antonov, L.; Yamada, S.; Ohta, K.; Yoshimura, T.; Tahara, K.; Inaba, A.; Sonoda, M.; Tobe, Y. Two-Photon Absorption Properties of Dehydrobenzo[12]annulenes and Hexakis(phenylethynyl)benzenes: Effect of Edge-Linkage. *ChemPhysChem* **2007**, *8*, 2671–2677.
- (43) Koning, R.; Zandstra, P. MCD and absorption spectra of tribenzo [12] annulene. *Chemical Physics* **1977**, *20*, 53–59.

- (44) Campbell, I.; Eglinton, G.; Henderson, W.; Raphael, R. 1, 2; 5, 6; 9, 10-Tribenzocyclododeca-1, 5, 9-triene-3, 7, 11-triyne and 1, 2; 5, 6; 9, 10; 13, 14-tetrabenzocyclohexadeca-1, 5, 9, 13-tetraene-3, 7, 11, 15-tetrayne. *Chemical Communications (London)* **1966**, 87–89.
- (45) Yoshimura, T.; Inaba, A.; Sonoda, M.; Tahara, K.; Tobe, Y.; Williams, R. V. Synthesis and Properties of Trefoil-Shaped Tris (hexadehydrotribenzo [12] annulene) and Tris (tetradehydrotribenzo [12] annulene). *Organic letters* **2006**, *8*, 2933–2936.
- (46) Johnson, C. A.; Lu, Y.; Haley, M. M. Carbon Networks Based on Benzocyclynes. 6. Synthesis of Graphyne Substructures via Directed Alkyne Metathesis. *Organic letters* **2007**, *9*, 3725–3728.
- (47) Tahara, K.; Yoshimura, T.; Ohno, M.; Sonoda, M.; Tobe, Y. Syntheses and Photophysical Properties of Boomerang-shaped Bis (dehydrobenzo [12] annulene) and Trapezoid-shaped Tris (dehydrobenzo [12] annulene). *Chemistry letters* **2007**, *36*, 838–839.
- (48) Iyoda, M.; Sirinintasak, S.; Nishiyama, Y.; Vorasingha, A.; Sultana, F.; Nakao, K.; Kuwatani, Y.; Matsuyama, H.; Yoshida, M.; Miyake, Y. Copper-Mediated Simple and Efficient Synthesis of Tribenzohexadehydro [12] annulene and Its Derivatives. *Synthesis* **2004**, *2004*, 1527–1531.
- (49) Sonoda, M.; Sakai, Y.; Yoshimura, T.; Tobe, Y.; Kamada, K. Convenient synthesis and photophysical properties of tetrabenzopentakisdehydro [12] annuleno [12] annulene. *Chemistry letters* **2004**, *33*, 972–973.

TOC Graphic



Supporting Information

Tunable Optoelectronic Properties of Triply-Bonded Carbon Molecules with Linear and Graphyne Substructures

Deepak Kumar Rai,[†] Himanshu Chakraborty,^{†,‡} and Alok Shukla^{*,†,¶}

[†]*Department of Physics, Indian Institute of Technology Bombay, Powai, Mumbai-400076,
INDIA.*

[‡]*Present Address: Department of Chemistry, Temple University, SERC 701E, 1925 N.
12th Street, Philadelphia, PA 19122, USA*

[¶]*Present Address: Department of Physics, School of Engineering and Applied Sciences,
Bennett University, Plot No 8-11, TechZone II, Greater Noida 201310 (UP), INDIA*

E-mail: shukla@phy.iitb.ac.in

In the following tables, we present detailed information about the excited states obtained in our calculations of optical absorption of various linear and graphyne substructures. The information includes the symmetries of various excited states, their excitation energies, dominant terms in their many-body wave-functions, and their transition dipole matrix elements with respect to the ground state, for all the molecules considered in this work.. The coefficient of charge conjugate of a given configuration in the many body wave function is abbreviated as 'c.c.', while the sign (+/-) preceding 'c.c.' indicates that the two coefficients have (same/opposite) signs. Note that for all the linear substructures the symmetry group is D_{2h} , while for the graphyne substructures, the symmetry group is specified in the caption.

Table S1: Excited states giving rise to peaks in the singlet linear absorption spectrum of LU-14, computed using the FCI approach, and the screened parameters in the PPP model. Subscripts x and y on a peak label, indicate the polarization direction of the absorbed photon.

Peak	Symmetry	Energy (eV)	Transition Dipole (\AA)	Dominant configurations in the many-body wave function
I_x	${}^1B_{3u}$	4.15	1.857	$ H \rightarrow L\rangle$ (-0.9184) $ H \rightarrow L + 2; H - 1 \rightarrow L\rangle$ (0.1095)
II_y	${}^1B_{2u}$	5.23	0.919	$ H \rightarrow L + 1\rangle$ -c.c.(0.6347) $ H \rightarrow L; H - 2 \rightarrow L\rangle$ +c.c.(0.0668)
III_x	${}^1B_{3u}$	6.25	1.001	$ H - 2 \rightarrow L + 2\rangle$ (-0.6122) $ H - 1 \rightarrow L + 1\rangle$ (0.5768)
IV_y	${}^1B_{2u}$	6.46	1.187	$ H - 3 \rightarrow L + 2\rangle$ +c.c.(0.6251) $ H \rightarrow L; H - 1 \rightarrow L + 3\rangle$ +c.c.(0.0783)
V_x	${}^1B_{3u}$	6.85	0.534	$ H - 4 \rightarrow L\rangle$ +c.c.(0.5274) $ H - 3 \rightarrow L + 3\rangle$ (0.4100)
VI_y	${}^1B_{2u}$	7.49	0.524	$ H - 1 \rightarrow L + 4\rangle$ -c.c.(0.5047) $ H \rightarrow L; H - 2 \rightarrow L\rangle$ +c.c.(0.2895)
VII_x	${}^1B_{3u}$	8.48	0.216	$ H \rightarrow L; H \rightarrow L + 3\rangle$ +c.c.(0.4907) $ H - 3 \rightarrow L + 3; H \rightarrow L + 3\rangle$ +c.c.(0.2356)

Table S2: Excited states giving rise to peaks in the singlet linear absorption spectrum of LU-14, computed using the FCI approach, and the standard parameters in the PPP model. Subscripts x and y on a peak label, indicate the polarization direction of the absorbed photon.

Peak	Symmetry	Energy (eV)	Transition Dipole (\AA)	Dominant configurations in the many-body wave function
I_x	${}^1B_{3u}$	4.15	1.706	$ H \rightarrow L\rangle$ (0.9173) $ H - 3 \rightarrow L + 3\rangle$ (0.2133)
II_x	${}^1B_{3u}$	5.65	1.214	$ H - 1 \rightarrow L + 1\rangle$ (-0.6012) $ H - 2 \rightarrow L + 2\rangle$ (0.5981)
III_y	${}^1B_{2u}$	5.81	1.136	$ H \rightarrow L + 1\rangle$ -c.c.(0.6332) $ H \rightarrow L; H - 1 \rightarrow L + 3\rangle$ +c.c.(0.1211)
IV_y	${}^1B_{2u}$	7.07	1.122	$ H - 3 \rightarrow L + 2\rangle$ +c.c.(0.5702) $ H - 4 \rightarrow L + 1\rangle$ -c.c.(0.2488)
V_y	${}^1B_{2u}$	8.79	0.253	$ H - 2 \rightarrow L + 5\rangle$ +c.c.(0.3152) $ H - 1 \rightarrow L + 6\rangle$ -c.c.(0.2974)

Table S3: Excited states giving rise to peaks in the singlet linear absorption spectrum of LU-22, computed using the QCI approach, and the screened parameters in the PPP model. Subscripts x and y on a peak label, indicate the polarization direction of the absorbed photon.

Peak	Symmetry	Energy (eV)	Transition Dipole (\AA)	Dominant configurations in the many-body wave function
I_x	${}^1B_{3u}$	3.85	2.4365	$ H \rightarrow L\rangle$ (0.8965) $ H \rightarrow L; H - 2 \rightarrow L + 3; H - 3 \rightarrow L + 2\rangle$ (0.0892)
II_y	${}^1B_{2u}$	5.28	0.7875	$ H \rightarrow L + 2\rangle - c.c.$ (0.6168) $ H \rightarrow L; H - 1 \rightarrow L + 2\rangle - c.c.$ (0.0721)
III_x	${}^1B_{3u}$	5.49	1.0849	$ H - 1 \rightarrow L + 1\rangle$ (0.8628) $ H - 4 \rightarrow L + 4\rangle$ (0.1196)
IV_y	${}^1B_{2u}$	6.12	0.9006	$ H - 3 \rightarrow L + 1\rangle + c.c.$ (0.6121) $ H \rightarrow L; H - 1 \rightarrow L + 2\rangle - c.c.$ (0.0792)
V_x	${}^1B_{3u}$	6.56	0.9131	$ H - 4 \rightarrow L + 4\rangle$ (0.7024) $ H - 2 \rightarrow L + 2\rangle$ (0.2761)
VI_y	${}^1B_{2u}$	6.94	1.0295	$ H - 5 \rightarrow L + 2\rangle + c.c.$ (0.5646) $ H - 4 \rightarrow L + 5\rangle + c.c.$ (0.2014)
VII_x	${}^1B_{3u}$	7.26	0.3502	$ H \rightarrow L; H - 1 \rightarrow L\rangle - c.c.$ (0.4335) $ H \rightarrow L + 1; H - 1 \rightarrow L + 1\rangle - c.c.$ (0.2644)
$VIII_y$	${}^1B_{2u}$	7.64	0.5912	$ H - 6 \rightarrow L + 3\rangle - c.c.$ (0.5660) $ H \rightarrow L; H - 3 \rightarrow L + 5\rangle - c.c.$ (0.1050)

Table S4: Excited states giving rise to peaks in the singlet linear absorption spectrum of LU-22, computed using the QCI approach, and the standard parameters in the PPP model. Subscripts x and y on a peak label, indicate the polarization direction of the absorbed photon.

Peak	Symmetry	Energy (eV)	Transition Dipole (\AA)	Dominant configurations in the many-body wave function
I_x	${}^1B_{3u}$	3.72	2.4532	$ H \rightarrow L\rangle$ (0.8742) $ H - 1 \rightarrow L + 1\rangle$ (0.2690)
II_x	${}^1B_{3u}$	5.18	0.2707	$ H - 1 \rightarrow L + 1\rangle$ (0.4376) $ H - 5 \rightarrow L\rangle - c.c.$ (0.4085)
$III_{x\&y}$	${}^1B_{3u}$	5.75	1.4725	$ H - 4 \rightarrow L + 4\rangle$ (0.6355) $ H - 2 \rightarrow L + 2\rangle$ (0.4071)
	${}^1B_{2u}$	5.79	1.1630	$ H \rightarrow L + 2\rangle - c.c.$ (0.5673) $ H - 3 \rightarrow L + 1\rangle + c.c.$ (0.2566)
IV_x	${}^1B_{3u}$	6.25	0.5583	$ H - 1 \rightarrow L + 1\rangle$ (0.6601) $ H \rightarrow L\rangle$ (0.2454)
V_x	${}^1B_{3u}$	6.59	0.3829	$ H - 4 \rightarrow L + 4\rangle$ (0.4210) $ H - 5 \rightarrow L\rangle - c.c.$ (0.3899)
VI_y	${}^1B_{2u}$	6.84	1.0462	$ H - 1 \rightarrow L + 3\rangle + c.c.$ (0.4693) $ H - 2 \rightarrow L + 5\rangle + c.c.$ (0.3080)
VII_x	${}^1B_{3u}$	7.36	0.6389	$ H - 6 \rightarrow L + 1\rangle + c.c.$ (0.3790) $ H - 5 \rightarrow L + 5\rangle$ (0.3557)
$VIII_y$	${}^1B_{2u}$	7.55	0.6961	$ H - 6 \rightarrow L + 3\rangle + c.c.$ (0.3496)
				$ H - 2 \rightarrow L + 5\rangle + c.c.$ (0.3152)

Table S5: Excited states giving rise to peaks in the singlet linear absorption spectrum of LU-30, computed using the MRSDCI approach, and the screened parameters in the PPP model. Subscripts x and y on a peak label, indicate the polarization direction of the absorbed photon.

Peak	Symmetry	Energy (eV)	Transition Dipole (\AA)	Dominant configurations in the many-body wave function
I_x	${}^1B_{3u}$	3.17	3.1340	$ H \rightarrow L\rangle$ (0.8794) $ H - 1 \rightarrow L + 1\rangle$ (0.1160)
II_x	${}^1B_{3u}$	4.40	1.3504	$ H - 2 \rightarrow L\rangle - c.c.$ (0.5382) $ H \rightarrow L; H \rightarrow L + 1\rangle + c.c.$ (0.2245)
III_y	${}^1B_{2u}$	4.75	0.9047	$ H - 5 \rightarrow L\rangle + c.c.$ (0.6021) $ H - 3 \rightarrow L\rangle - c.c.$ (0.1223)
IV_y	${}^1B_{2u}$	5.27	0.5107	$ H - 6 \rightarrow L + 1\rangle + c.c.$ (0.5969) $ H - 5 \rightarrow L + 2\rangle + c.c.$ (0.1322)
V_y	${}^1B_{2u}$	5.52	0.7990	$ H - 1 \rightarrow L + 4\rangle - c.c.$ (0.5924) $ H - 3 \rightarrow L\rangle - c.c.$ (0.1237)
VI_x	${}^1B_{3u}$	5.70	0.9414	$ H - 2 \rightarrow L + 2\rangle$ (0.7722) $ H - 1 \rightarrow L + 7\rangle - c.c.$ (0.2515)
VII_y	${}^1B_{2u}$	5.90	0.5372	$ H - 2 \rightarrow L + 5\rangle + c.c.$ (0.5761) $ H - 3 \rightarrow L + 2\rangle - c.c.$ (0.1397)
$VIII_y$	${}^1B_{2u}$	6.16	0.8866	$ H - 3 \rightarrow L + 2\rangle - c.c.$ (0.5818) $ H - 2 \rightarrow L + 5\rangle + c.c.$ (0.1411)
$VIII_x$	${}^1B_{3u}$	6.28	1.2497	$ H - 5 \rightarrow L + 5\rangle$ (0.4855) $ H - 6 \rightarrow L + 6\rangle$ (0.4710)
IX_y	${}^1B_{2u}$	6.64	0.9095	$ H - 6 \rightarrow L + 7\rangle - c.c.$ (0.5897) $ H - 7 \rightarrow L + 4\rangle + c.c.$ (0.1054)
X_y	${}^1B_{2u}$	6.81	0.9317	$ H - 7 \rightarrow L + 4\rangle + c.c.$ (0.5387) $ H - 8 \rightarrow L + 3\rangle - c.c.$ (0.1984)
XI_y	${}^1B_{2u}$	7.39	0.5054	$ H - 8 \rightarrow L + 3\rangle - c.c.$ (0.5325) $ H - 7 \rightarrow L + 4\rangle + c.c.$ (0.1957)

Table S6: Continued from previous table: excited states giving rise to peaks in the singlet linear absorption spectrum of LU-30, computed using the MRSDCI approach, and the screened parameters in the PPP model. Subscripts x and y on a peak label, indicate the polarization direction of the absorbed photon.

Peak	Symmetry	Energy (eV)	Transition Dipole (\AA)	Dominant configurations in the many-body wave function
XII_y	${}^1B_{2u}$	7.74	0.6741	$ H - 9 \rightarrow L + 6\rangle + c.c.$ (0.5434) $ H - 10 \rightarrow L + 5\rangle + c.c.$ (0.5434)
$XIII_y$	${}^1B_{2u}$	8.27	0.3430	$ H - 5 \rightarrow L + 10\rangle + c.c.$ (0.5143) $ H - 6 \rightarrow L + 9\rangle + c.c.$ (0.2058)
$XIII_x$	${}^1B_{3u}$	8.36	0.1910	$ H - 8 \rightarrow L + 8\rangle$ (0.6756) $ H - 14 \rightarrow L\rangle + c.c.$ (0.2105)

Table S7: Excited states giving rise to peaks in the singlet linear absorption spectrum of LU-30, computed using the MRSDCI approach, and the standard parameters in the PPP model. Subscripts x and y on a peak label, indicate the polarization direction of the absorbed photon.

Peak	Symmetry	Energy (eV)	Transition Dipole (\AA)	Dominant configurations in the many-body wave function
I_x	${}^1B_{3u}$	3.36	3.0352	$ H \rightarrow L\rangle$ (0.8282)
II_x	${}^1B_{3u}$	4.67	0.6637	$ H - 1 \rightarrow L + 1\rangle$ (0.3202)
III_y	${}^1B_{2u}$	5.67	1.1687	$ H - 1 \rightarrow L + 1\rangle$ (0.4857) $ H - 2 \rightarrow L\rangle + c.c.$ (0.4590)
III_x	${}^1B_{3u}$	5.73	1.4541	$ H - 3 \rightarrow L\rangle + c.c.$ (0.4863) $ H - 1 \rightarrow L + 4\rangle - c.c.$ (0.3495)
IV_y	${}^1B_{2u}$	6.64	0.9854	$ H - 1 \rightarrow L + 1\rangle$ (0.3925) $ H - 6 \rightarrow L + 6\rangle$ (0.3781)
IV_x	${}^1B_{3u}$	6.66	0.6069	$ H - 2 \rightarrow L + 3\rangle + c.c.$ (0.3490) $ H - 4 \rightarrow L + 1\rangle - c.c.$ (0.3238)
V_y	${}^1B_{2u}$	6.90	0.7320	$ H - 2 \rightarrow L + 2\rangle$ (0.3691) $ H - 4 \rightarrow L + 4\rangle$ (0.3584)
VI_y	${}^1B_{2u}$	7.26	0.8099	$ H - 2 \rightarrow L + 5\rangle - c.c.$ (0.4193) $ H - 6 \rightarrow L + 1\rangle + c.c.$ (0.2236)
VII_x	${}^1B_{3u}$	7.40	0.6628	$ H - 4 \rightarrow L + 7\rangle + c.c.$ (0.3316) $ H - 1 \rightarrow L + 4\rangle - c.c.$ (0.2479)
$VIII_y$	${}^1B_{2u}$	7.54	0.7710	$ H - 3 \rightarrow L + 7\rangle$ (0.3319) $ H - 9 \rightarrow L + 1\rangle - c.c.$ (0.3136)
IX_y	${}^1B_{2u}$	8.65	0.2544	$ H - 6 \rightarrow L + 7\rangle - c.c.$ (0.4205) $ H - 8 \rightarrow L + 5\rangle + c.c.$ (0.2672) $ H - 6 \rightarrow L + 9\rangle - c.c.$ (0.2390) $ H - 10 \rightarrow L + 5\rangle + c.c.$ (0.1584)

Table S8: Excited states giving rise to peaks in the singlet linear absorption spectrum of LU-38, computed using the MRSDCI approach, and the screened parameters in the PPP model. Subscripts x and y on a peak label, indicate the polarization direction of the absorbed photon.

Peak	Symmetry	Energy (eV)	Transition Dipole (\AA)	Dominant configurations in the many-body wave function
I_x	${}^1B_{3u}$	3.04	3.567	$ H \rightarrow L\rangle$ (0.8590) $ H - 1 \rightarrow L + 1\rangle$ (0.1596)
II_x	${}^1B_{3u}$	3.98	1.549	$ H - 1 \rightarrow L + 1\rangle$ (0.7112) $ H \rightarrow L + 2\rangle + c.c.$ (0.3535)
III_x	${}^1B_{3u}$	4.21	0.6461	$ H \rightarrow L + 2\rangle + c.c.$ (0.4997) $ H - 1 \rightarrow L + 1\rangle$ (0.4650)
IV_y	${}^1B_{2u}$	4.80	0.8975	$ H - 6 \rightarrow L\rangle - c.c.$ (0.4255) $ H - 8 \rightarrow L\rangle + c.c.$ (0.4181)
V_x	${}^1B_{3u}$	5.00	0.9116	$ H - 2 \rightarrow L + 2\rangle$ (0.6663) $ H - 1 \rightarrow L + 3\rangle + c.c.$ (0.3837)
$VI_{x\&y}$	${}^1B_{3u}$	5.18	0.5733	$ H - 2 \rightarrow L + 2\rangle$ (0.5235) $ H - 1 \rightarrow L + 3\rangle + c.c.$ (0.4520)
	${}^1B_{2u}$	5.24	0.6804	$ H - 1 \rightarrow L + 7\rangle - c.c.$ (0.5687) $ H - 2 \rightarrow L + 6\rangle - c.c.$ (0.1425)
VII_y	${}^1B_{2u}$	5.41	0.6612	$ H - 5 \rightarrow L + 1\rangle + c.c.$ (0.5415) $ H - 4 \rightarrow L\rangle - c.c.$ (0.2384)
$VIII_y$	${}^1B_{2u}$	5.74	0.6238	$ H - 6 \rightarrow L + 2\rangle - c.c.$ (0.4486) $ H - 2 \rightarrow L + 8\rangle + c.c.$ (0.4107)
IX_y	${}^1B_{2u}$	5.91	0.7893	$ H - 4 \rightarrow L + 2\rangle - c.c.$ (0.5654) $ H - 5 \rightarrow L + 1\rangle + c.c.$ (0.1576)
X_x	${}^1B_{3u}$	6.16	1.222	$ H - 3 \rightarrow L + 3\rangle$ (0.3874) $ H - 10 \rightarrow L + 1\rangle + c.c.$ (0.3254)

Table S9: Continued from previous table: excited states giving rise to peaks in the singlet linear absorption spectrum of LU-38, computed using the MRSDCI approach, and the screened parameters in the PPP model. Subscripts x and y on a peak label, indicate the polarization direction of the absorbed photon.

Peak	Symmetry	Energy (eV)	Transition Dipole (\AA)	Dominant configurations in the many-body wave function
$XI_{x\&y}$	${}^1B_{2u}$	6.28	0.6922	$ H - 3 \rightarrow L + 7\rangle + c.c.(0.5641)$ $ H - 2 \rightarrow L + 8\rangle + c.c.(0.1209)$
	${}^1B_{3u}$	6.36	0.8594	$ H - 5 \rightarrow L + 5\rangle(0.4034)$ $ H - 4 \rightarrow L + 4\rangle(0.4028)$
XII_y	${}^1B_{2u}$	6.44	0.8576	$ H - 3 \rightarrow L + 5\rangle + c.c.(0.5579)$ $ H - 9 \rightarrow L + 4\rangle + c.c.(0.1768)$
$XIII_y$	${}^1B_{2u}$	6.82	0.9093	$ H - 8 \rightarrow L + 9\rangle - c.c.(0.5582)$ $ H - 7 \rightarrow L + 10\rangle - c.c.(0.1647)$
XIV_y	${}^1B_{2u}$	6.96	0.7979	$ H - 9 \rightarrow L + 4\rangle + c.c.(0.5220)$ $ H - 10 \rightarrow L + 5\rangle + c.c.(0.2279)$
XV_y	${}^1B_{2u}$	7.47	0.4714	$ H - 10 \rightarrow L + 5\rangle + c.c.(0.5023)$ $ H - 9 \rightarrow L + 4\rangle + c.c.(0.2365)$
XVI_y	${}^1B_{2u}$	8.01	0.2660	$ H - 11 \rightarrow L + 4\rangle + c.c.(0.5707)$
				$ H - 10 \rightarrow L + 5\rangle + c.c.(0.2224)$

Table S10: Excited states giving rise to peaks in the singlet linear absorption spectrum of LU-38, computed using the MRSDCI approach, and the standard parameters in the PPP model. Subscripts x and y on a peak label, indicate the polarization direction of the absorbed photon.

Peak	Symmetry	Energy (eV)	Transition Dipole (\AA)	Dominant configurations in the many-body wave function
I_x	${}^1B_{3u}$	3.26	3.506	$ H \rightarrow L\rangle$ (0.7786) $ H - 1 \rightarrow L + 1\rangle$ (0.3600)
II_x	${}^1B_{3u}$	4.28	0.8780	$ H \rightarrow L + 2\rangle + c.c.$ (0.4708) $ H - 1 \rightarrow L + 1\rangle$ (0.4699)
$III_{x\&y}$	${}^1B_{2u}$	5.61	1.3281	$ H \rightarrow L + 6\rangle - c.c.$ (0.5487) $ H - 1 \rightarrow L + 7\rangle + c.c.$ (0.2555)
	${}^1B_{3u}$	5.68	1.533	$ H - 6 \rightarrow L + 6\rangle$ (0.4756) $ H - 8 \rightarrow L + 8\rangle$ (0.4701)
IV_y	${}^1B_{2u}$	5.81	1.275	$ H \rightarrow L + 4\rangle - c.c.$ (0.4002) $ H - 5 \rightarrow L + 1\rangle - c.c.$ (0.3965)
$V_{x\&y}$	${}^1B_{2u}$	6.17	0.3747	$ H - 7 \rightarrow L + 1\rangle + c.c.$ (0.3272) $ H - 8 \rightarrow L + 2\rangle - c.c.$ (0.2999)
	${}^1B_{3u}$	6.33	0.3915	$ H - 2 \rightarrow L + 2\rangle$ (0.4988) $ H - 3 \rightarrow L + 1\rangle - c.c.$ (0.2390)
$VI_{x\&y}$	${}^1B_{3u}$	6.71	0.3954	$ H - 2 \rightarrow L + 2\rangle$ (0.3526) $ H - 3 \rightarrow L + 3\rangle$ (0.2556)
	${}^1B_{2u}$	6.79	0.9557	$ H \rightarrow L + 4\rangle - c.c.$ (0.3641) $ H - 4 \rightarrow L + 2\rangle + c.c.$ (0.3119)
$VII_{x\&y}$	${}^1B_{3u}$	6.83	0.4546	$ H - 9 \rightarrow L + 2\rangle + c.c.$ (0.3409) $ H - 5 \rightarrow L + 5\rangle$ (0.2625)
	${}^1B_{2u}$	6.89	0.3119	$ H - 7 \rightarrow L + 3\rangle - c.c.$ (0.3193) $ H - 1 \rightarrow L + 7\rangle + c.c.$ (0.2858)
$VIII_y$	${}^1B_{2u}$	7.32	0.7362	$ H - 1 \rightarrow L + 5\rangle - c.c.$ (0.3158) $ H - 3 \rightarrow L + 5\rangle + c.c.$ (0.2532)

Table S11: Continued from previous table: excited states giving rise to peaks in the singlet linear absorption spectrum of LU-38, computed using the MRSDCI approach, and the standard parameters in the PPP model. Subscripts x and y on a peak label, indicate the polarization direction of the absorbed photon.

Peak	Symmetry	Energy (eV)	Transition Dipole (\AA)	Dominant configurations in the many-body wave function
$IX_{x\&y}$	${}^1B_{3u}$	7.47	0.6369	$ H - 10 \rightarrow L + 3\rangle - c.c.(0.2859)$ $ H - 11 \rightarrow L + 2\rangle + c.c.(0.2814)$
	${}^1B_{2u}$	7.54	0.7875	$ H - 3 \rightarrow L + 7\rangle - c.c.(0.2664)$ $ H - 8 \rightarrow L + 9\rangle - c.c.(0.2573)$
X_y	${}^1B_{2u}$	6.16	0.3268	$ H - 10 \rightarrow L + 7\rangle + c.c.(0.3640)$ $ H - 2 \rightarrow L + 8\rangle - c.c.(0.1897)$
XI_y	${}^1B_{2u}$	6.28	0.2620	$ H - 11 \rightarrow L + 8\rangle - c.c.(0.2017)$ $ H - 3 \rightarrow L + 7\rangle - c.c.(0.2015)$
XII_y	${}^1B_{2u}$	6.44	0.4128	$ H - 12 \rightarrow L + 7\rangle - c.c.(0.3573)$ $ H - 9 \rightarrow L + 8\rangle + c.c.(0.2410)$

Table S12: Excited states giving rise to peaks in the singlet linear absorption spectrum of GU-24 (D_{3h} symmetry), computed using the QCI approach, and the screened parameters in the PPP model. Due to the symmetry, several orbitals are degenerate, and those degeneracies are indicated by means of subscripts 1, 2 etc. DF indicates a dipole forbidden excited state. Subscripts x and y on a peak label, indicate the polarization direction of the absorbed photon.

Peak	Symmetry	Energy (eV)	Transition Dipole (\AA)	Dominant configurations in the many-body wave function
DF	${}^1A_2''$	3.15	0.000	$ H \rightarrow L\rangle$ (0.8957) $ H \rightarrow L; (H-1)_2 \rightarrow (L+1)_1\rangle - c.c.$ (0.0488)
DF	${}^1E'$	3.48	0.000	$ H \rightarrow (L+1)_1\rangle + c.c.$ (0.5408) $ H \rightarrow (L+3)_2\rangle - c.c.$ (0.1225)
	${}^1E'$	3.48	0.000	$ H \rightarrow (L+1)_2\rangle + c.c.$ (0.5408) $ H \rightarrow (L+3)_1\rangle + c.c.$ (0.1225)
$I_{x\&y}$	${}^1E'$	4.32	2.102	$ H \rightarrow (L+1)_2\rangle - c.c.$ (0.6255) $ H \rightarrow L; (H-1)_2 \rightarrow (L+1)_2; (H-1)_2 \rightarrow L\rangle - c.c.$ (0.0488)
	${}^1E'$	4.32	2.102	$ H \rightarrow (L+1)_1\rangle - c.c.$ (0.6255)
$II_{x\&y}$	${}^1E'$	5.12	0.669	$ H \rightarrow L; (H-1)_1 \rightarrow (L+1)_1; (H-1)_1 \rightarrow L\rangle - c.c.$ (0.0488) $ (H-1)_2 \rightarrow (L+1)_1\rangle + c.c.$ (0.5915)
	${}^1E'$	5.12	0.669	$ (H-3)_1 \rightarrow L\rangle - c.c.$ (0.1553) $ (H-1)_1 \rightarrow (L+1)_1\rangle$ (-0.5920)
$III_{x\&y}$	${}^1E'$	6.12	0.728	$ (H-1)_2 \rightarrow (L+1)_2\rangle$ (0.5910) $ (H-3)_1 \rightarrow (L+1)_1\rangle + c.c.$ (0.3507)
	${}^1E'$	6.12	0.728	$ (H-3)_2 \rightarrow (L+1)_2\rangle - c.c.$ (0.3507) $ (H-3)_1 \rightarrow (L+1)_2\rangle + c.c.$ (0.3507)
$IV_{x\&y}$	${}^1E'$	6.54	0.193	$ (H-3)_2 \rightarrow (L+1)_1\rangle - c.c.$ (0.3507) $ (H-5)_2 \rightarrow L\rangle + c.c.$ (0.5327)
	${}^1E'$	6.54	0.193	$ H-4 \rightarrow (L+1)_2\rangle - c.c.$ (0.1170) $ H \rightarrow (L+5)_1\rangle - c.c.$ (0.5327) $ (H-1)_1 \rightarrow L; (H-1)_2 \rightarrow L\rangle + c.c.$ (0.1173)

Table S13: Excited states giving rise to peaks in the singlet linear absorption spectrum of GU-24 (D_{3h} symmetry), computed using the QCI approach, and the standard parameters in the PPP model. Due to the symmetry, several orbitals are degenerate, and those degeneracies are indicated by means of subscripts 1, 2 etc. DF indicates a dipole forbidden excited state. Subscripts x and y on a peak label, indicate the polarization direction of the absorbed photon.

Peak	Symmetry	Energy (eV)	Transition Dipole (\AA)	Dominant configurations in the many-body wave function
DF	${}^1A_2''$	2.85	0.000	$ H \rightarrow L\rangle$ (0.8912) $ (H-1)_2 \rightarrow (L+1)_2 \rangle + c.c.$ (0.1124)
DF	${}^1E'$	3.72	0.000	$ H \rightarrow (L+1)_1\rangle - c.c.$ (0.5292) $ H \rightarrow (L+3)_2\rangle + c.c.$ (0.1487)
	${}^1E'$	3.72	0.000	$ H \rightarrow (L+1)_2\rangle - c.c.$ (0.5292) $ H \rightarrow (L+3)_1\rangle + c.c.$ (0.1487)
$I_{X\&y}$	${}^1E'$	4.38	2.053	$ H \rightarrow (L+1)_2\rangle + c.c.$ (0.6153) $ (H-1)_2 \rightarrow (L+1)_1 \rangle + c.c.$ (0.1173)
	${}^1E'$	4.38	2.053	$ (H-1)_1 \rightarrow L \rangle + c.c.$ (0.6153) $ (H-1)_2 \rightarrow (L+1)_2 \rangle - c.c.$ (0.1173)
$II_{x\&y}$	${}^1E'$	5.21	0.723	$ (H-3)_1 \rightarrow L \rangle - c.c.$ (0.4385) $ (H-2) \rightarrow (L+1)_1 \rangle + c.c.$ (0.2898)
	${}^1E'$	5.21	0.723	$ (H-3)_2 \rightarrow L \rangle - c.c.$ (0.4385) $ (H-2) \rightarrow (L+1)_2 \rangle + c.c.$ (0.2898)
$III_{X\&y}$	${}^1E'$	5.99	1.103	$ (H-1)_2 \rightarrow L+2 \rangle + c.c.$ (0.3475) $ (H-3)_2 \rightarrow L \rangle - c.c.$ (0.3287)
	${}^1E'$	5.99	1.103	$ H-2 \rightarrow (L+1)_1\rangle + c.c.$ (0.3475) $ (H-3)_1 \rightarrow L \rangle - c.c.$ (0.3287)
$IV_{x\&y}$	${}^1E'$	7.37	0.866	$ (H-3)_2 \rightarrow (L+3)_2 \rangle - c.c.$ (0.3243) $ (H-1)_1 \rightarrow L+4 \rangle + c.c.$ (0.2816)
	${}^1E'$	7.37	0.866	$ (H-3)_1 \rightarrow (L+3)_2 \rangle + c.c.$ (0.3243) $ (H-1)_2 \rightarrow L+4 \rangle + c.c.$ (0.2816)

Table S14: Excited states giving rise to peaks in the singlet linear absorption spectrum of GU-34 (D_{2h} symmetry), computed using the MRSDCI approach, and the screened parameters in the PPP model. Subscripts x and y on a peak label, indicate the polarization direction of the absorbed photon.

Peak	Symmetry	Energy (eV)	Transition Dipole (\AA)	Dominant configurations in the many-body wave function
I_x	$^1B_{3u}$	2.37	0.305	$ H \rightarrow L\rangle$ (-0.8716) $ H - 1 \rightarrow L + 1\rangle$ (0.0998)
II_x	$^1B_{3u}$	3.34	1.572	$ H - 1 \rightarrow L + 1\rangle$ (0.8652) $ H \rightarrow L\rangle$ (0.0922)
III_y	$^1B_{2u}$	3.51	2.604	$ H - 2 \rightarrow L\rangle + c.c.$ (0.6148) $ H \rightarrow L + 3; H \rightarrow L + 2\rangle - c.c.$ (0.0494)
$IV_{x\&y}$	$^1B_{3u}$	4.18	2.025	$ H - 4 \rightarrow L\rangle + c.c.$ (0.6108) $ H - 2 \rightarrow L + 2\rangle$ (-0.0643)
	$^1B_{2u}$	4.23	2.118	$ H - 1 \rightarrow L + 3\rangle + c.c.$ (0.6066) $ H - 3 \rightarrow L + 1; H - 2 \rightarrow L + 1\rangle - c.c.$ (0.0580)
V_y	$^1B_{2u}$	5.00	0.732	$ H - 1 \rightarrow L + 6\rangle + c.c.$ (0.5046) $ H - 4 \rightarrow L + 6\rangle + c.c.$ (0.3249)
VI_x	$^1B_{3u}$	5.57	0.668	$ H - 2 \rightarrow L + 5\rangle - c.c.$ (0.4440) $ H \rightarrow L; H - 3 \rightarrow L\rangle - c.c.$ (0.3192)
$VII_{x\&y}$	$^1B_{3u}$	6.00	0.378	$ H - 6 \rightarrow L + 3\rangle + c.c.$ (0.5671) $ H - 1 \rightarrow L + 1; H \rightarrow L + 3\rangle + c.c.$ (0.1040)
	$^1B_{2u}$	6.09	0.128	$ H - 7 \rightarrow L + 3\rangle - c.c.$ (0.3660) $ H - 2 \rightarrow L + 1; H - 2 \rightarrow L\rangle - c.c.$ (0.2364)
$VIII_x$	$^1B_{3u}$	6.71	0.611	$ H - 6 \rightarrow L + 6\rangle$ (-0.3884) $ H \rightarrow L; H - 1 \rightarrow L + 5\rangle - c.c.$ (0.3004)
$IX_{x\&y}$	$^1B_{3u}$	6.95	0.785	$ H - 7 \rightarrow L + 7\rangle$ (0.5958) $ H - 9 \rightarrow L + 3\rangle + c.c.$ (0.2606)
	$^1B_{2u}$	6.86	0.449	$ H - 10 \rightarrow L + 2\rangle - c.c.$ (0.2746) $ H - 12 \rightarrow L\rangle + c.c.$ (0.2119)
X_y	$^1B_{2u}$	7.52	0.266	$ H - 3 \rightarrow L + 11\rangle + c.c.$ (0.3422) $ H \rightarrow L + 1; H - 1 \rightarrow L + 7\rangle - c.c.$ (0.2583)

Table S15: Excited states giving rise to peaks in the singlet linear absorption spectrum of GU-34 (D_{2h} symmetry), computed using the MRSDCI approach, and the standard parameters in the PPP model. Subscripts x and y on a peak label, indicate the polarization direction of the absorbed photon.

Peak	Symmetry	Energy (eV)	Transition Dipole (\AA)	Dominant configurations in the many-body wave function
I_x	$^1B_{3u}$	2.47	0.113	$ H \rightarrow L\rangle(0.8438)$ $ H - 1 \rightarrow L + 1\rangle(-0.2588)$
$II_{x\&y}$	$^1B_{3u}$	3.97	1.688	$ H - 1 \rightarrow L + 1\rangle(0.8076)$ $ H \rightarrow L\rangle(-0.2452)$
	$^1B_{2u}$	4.06	2.945	$ H - 2 \rightarrow L\rangle-c.c.(0.5857)$ $ H - 1 \rightarrow L + 3\rangle-c.c.(0.2121)$
III_x	$^1B_{3u}$	4.58	1.329	$ H \rightarrow L + 4\rangle+c.c.(0.5501)$ $ H - 7 \rightarrow L + 1\rangle-c.c.(0.2015)$
IV_y	$^1B_{2u}$	4.95	1.435	$ H - 1 \rightarrow L + 3\rangle-c.c.(0.5459)$ $ H - 2 \rightarrow L\rangle-c.c.(0.1719)$
V_x	$^1B_{3u}$	5.39	1.622	$ H - 7 \rightarrow L + 1\rangle-c.c.(0.3167)$ $ H - 5 \rightarrow L + 2\rangle+c.c.(0.3160)$
$VI_{x\&y}$	$^1B_{3u}$	5.96	0.490	$ H - 3 \rightarrow L + 3\rangle(0.3259)$ $ H - 1 \rightarrow L + 7\rangle-c.c.(0.3103)$
	$^1B_{2u}$	5.99	0.513	$ H - 2 \rightarrow L + 4\rangle-c.c.(0.4821)$ $ H - 1 \rightarrow L + 6\rangle-c.c.(0.2396)$
VII_x	$^1B_{3u}$	6.14	0.275	$ H - 8 \rightarrow L\rangle-c.c.(0.3488)$ $ H - 4 \rightarrow L + 4\rangle(-0.3196)$
$VIII_x$	$^1B_{3u}$	6.52	0.371	$ H - 4 \rightarrow L + 4\rangle(-0.3332)$ $ H \rightarrow L; H - 1 \rightarrow L + 2\rangle+c.c.(0.3141)$
IX_y	$^1B_{2u}$	6.87	0.610	$ H - 3 \rightarrow L + 7\rangle+c.c.(0.4236)$ $ H - 4 \rightarrow L + 5\rangle+c.c.(-0.3217)$

Table S16: Continued from the previous table: excited states giving rise to peaks in the singlet linear absorption spectrum of GU-34 (D_{2h} symmetry), computed using the MRSDCI approach, and the standard parameters in the PPP model. Subscripts x and y on a peak label, indicate the polarization direction of the absorbed photon.

Peak	Symmetry	Energy (eV)	Transition Dipole (\AA)	Dominant configurations in the many-body wave function
X_x	$^1B_{3u}$	7.26	0.910	$ H - 1 \rightarrow L + 11\rangle+c.c.(0.2628)$ $ H - 8 \rightarrow L + 4\rangle-c.c.(0.2406)$
$XI_{x\&y}$	$^1B_{2u}$	7.79	0.246	$ H - 6 \rightarrow L + 7\rangle-c.c.(0.2402)$ $ H \rightarrow L; H - 4 \rightarrow L + 1\rangle-c.c.(0.2076)$
	$^1B_{3u}$	7.84	0.283	$ H - 7 \rightarrow L + 7\rangle(0.3944)$ $ H - 5 \rightarrow L + 5\rangle(-0.2950)$

Table S17: Excited states giving rise to peaks in the singlet linear absorption spectrum of GU-42 (D_{2h} symmetry), computed using the MRSDCI approach, and the screened parameters in the PPP model. Subscripts x and y on a peak label, indicate the polarization direction of the absorbed photon.

Peak	Symmetry	E (eV)	Transition Dipole (Å)	Dominant configurations in the many-body wave function
I_x	${}^1B_{3u}$	2.43	0.402	$ H \rightarrow L\rangle$ (-0.8622)
II_y	${}^1B_{2u}$	3.38	3.165	$ H - 1 \rightarrow L + 1\rangle$ (-0.1552)
III_x	${}^1B_{3u}$	3.64	1.859	$ H - 2 \rightarrow L\rangle + c.c.$ (0.6128)
IV_x	${}^1B_{3u}$	3.81	1.991	$ H - 5 \rightarrow L\rangle - c.c.$ (0.0621)
V_x	${}^1B_{3u}$	4.55	1.765	$ H - 1 \rightarrow L + 1\rangle$ (0.8174)
VI_y	${}^1B_{2u}$	4.81	1.015	$ H \rightarrow L + 3\rangle + c.c.$ (0.1761)
VII_x	${}^1B_{3u}$	5.72	0.779	$ H \rightarrow L + 3\rangle + c.c.$ (0.5868)
$VIII_y$	${}^1B_{2u}$	5.87	0.728	$ H - 1 \rightarrow L + 1\rangle$ (0.2327)
IX_x	${}^1B_{3u}$	6.00	0.614	$ H - 4 \rightarrow L + 1\rangle - c.c.$ (0.5629)
X_y	${}^1B_{2u}$	6.22	0.641	$ H - 2 \rightarrow L + 2\rangle$ (-0.2515)
XI_y	${}^1B_{2u}$	6.92	0.246	$ H - 1 \rightarrow L + 5\rangle - c.c.$ (0.5948)
				$ H - 8 \rightarrow L\rangle + c.c.$ (0.1082)
				$ H - 2 \rightarrow L + 8\rangle + c.c.$ (0.5003)
				$ H - 5 \rightarrow L + 5\rangle$ (-0.3976)
				$ H - 3 \rightarrow L + 6\rangle - c.c.$ (0.3982)
				$ H \rightarrow L; H - 3 \rightarrow L + 1\rangle - c.c.$ (0.3178)
				$ H - 3 \rightarrow L + 9\rangle + c.c.$ (0.4878)
				$ H - 10 \rightarrow L + 1\rangle + c.c.$ (0.2210)
				$ H - 4 \rightarrow L + 7\rangle - c.c.$ (0.4329)
				$ H \rightarrow L + 14\rangle + c.c.$ (0.3011)
				$ H \rightarrow L; H - 9 \rightarrow L + 1\rangle - c.c.$ (0.3322)
				$ H - 1 \rightarrow L; H - 4 \rightarrow L + 1\rangle + c.c.$ (0.2573)

Table S18: Excited states giving rise to peaks in the singlet linear absorption spectrum of GU-42 (D_{2h} symmetry), computed using the MRSDCI approach, and the standard parameters in the PPP model. Subscripts x and y on a peak label, indicate the polarization direction of the absorbed photon.

Peak	Symmetry	Energy (eV)	Transition Dipole (\AA)	Dominant configurations in the many-body wave function
I_x	${}^1B_{3u}$	2.53	0.259	$ H \rightarrow L\rangle(-0.8111)$ $ H - 1 \rightarrow L + 1\rangle(-0.3222)$
II_y	${}^1B_{2u}$	3.72	3.138	$ H \rightarrow L + 2\rangle-c.c.(0.5902)$ $ H - 5 \rightarrow L + 1\rangle-c.c.(0.1705)$
III_x	${}^1B_{3u}$	4.13	2.572	$ H - 1 \rightarrow L + 1\rangle(0.5249)$ $ H \rightarrow L + 3\rangle-c.c.(0.4288)$
IV_x	${}^1B_{3u}$	4.57	0.578	$ H - 2 \rightarrow L + 2\rangle(0.4375)$ $ H - 1 \rightarrow L + 1\rangle(0.2865)$
V_x	${}^1B_{3u}$	4.87	0.985	$ H - 2 \rightarrow L + 2\rangle(0.5753)$ $ H - 1 \rightarrow L + 1\rangle(0.2865)$
VI_x	${}^1B_{3u}$	5.33	1.370	$ H - 1 \rightarrow L + 4\rangle-c.c.(0.3499)$ $ H - 2 \rightarrow L + 2\rangle(0.3242)$
$VII_{x\&y}$	${}^1B_{2u}$	5.90	1.113	$ H - 8 \rightarrow L\rangle+c.c.(0.4317)$ $ H - 3 \rightarrow L + 6\rangle-c.c.(0.2231)$
	${}^1B_{3u}$	5.96	0.971	$ H \rightarrow L + 9\rangle-c.c.(0.3947)$ $ H - 4 \rightarrow L + 4\rangle(-0.2747)$
$VIII_x$	${}^1B_{3u}$	6.11	0.943	$ H - 3 \rightarrow L + 3\rangle(-0.3502)$ $ H - 2 \rightarrow L + 8\rangle-c.c.(0.3367)$
IX_x	${}^1B_{3u}$	6.53	0.523	$ H - 4 \rightarrow L + 4\rangle(0.2678)$ $ H - 6 \rightarrow L + 2\rangle-c.c.(0.2528)$
X_y	${}^1B_{2u}$	6.79	0.655	$ H \rightarrow L; H - 3 \rightarrow L + 1\rangle+c.c.(0.2387)$ $ H - 3 \rightarrow L + 8\rangle-c.c.(0.2345)$

Table S19: Continued from the previous table: excited states giving rise to peaks in the singlet linear absorption spectrum of GU-42 (D_{2h} symmetry), computed using the MRSDCI approach, and the standard parameters in the PPP model. Subscripts x and y on a peak label, indicate the polarization direction of the absorbed photon.

Peak	Symmetry	Energy (eV)	Transition Dipole (\AA)	Dominant configurations in the many-body wave function
XI_y	${}^1B_{2u}$	6.92	0.577	$ H \rightarrow L; H - 3 \rightarrow L + 1\rangle + c.c.(0.3399)$ $ H - 7 \rightarrow L + 1\rangle - c.c.(0.2169)$
$XII_{x\&y}$	${}^1B_{3u}$	7.52	0.236	$ H - 5 \rightarrow L + 7\rangle + c.c.(0.3158)$ $ H - 8 \rightarrow L + 8\rangle (-0.2281)$
	${}^1B_{2u}$	7.57	0.533	$ H - 9 \rightarrow L + 6\rangle - c.c.(0.2619)$ $ H - 3 \rightarrow L + 6\rangle - c.c.(0.2064)$
$XIII_x$	${}^1B_{3u}$	8.02	0.5241	$ H - 9 \rightarrow L + 9\rangle (-0.3323)$ $ H - 2 \rightarrow L + 14\rangle - c.c.(0.2669)$

Table S20: Excited states giving rise to peaks in the singlet linear absorption spectrum of GU-42 (C_{2v} symmetry), computed using the MRSDCI approach, and the screened parameters in the PPP model. Subscripts x and y on a peak label, indicate the polarization direction of the absorbed photon.

Peak	Symmetry	Energy (eV)	Transition Dipole (\AA)	Dominant configurations in the many-body wave function
I_x	1B_1	2.87	2.176	$ H - 1 \rightarrow L + 1\rangle$ (0.750) $ H \rightarrow L\rangle$ (0.4331)
$II_{x\&y}$	1A_1	3.73	2.436	$ H \rightarrow L + 2\rangle - c.c.$ (0.6054) $ H - 3 \rightarrow L + 1\rangle + c.c.$ (0.1239)
	1B_1	3.75	2.101	$ H \rightarrow L + 3\rangle - c.c.$ (0.5444) $ H - 2 \rightarrow L + 1\rangle + c.c.$ (0.2469)
III_x	1B_1	4.17	1.137	$ H - 1 \rightarrow L + 4\rangle - c.c.$ (0.5909) $ H - 5 \rightarrow L\rangle - c.c.$ (0.1083)
IV_y	1A_1	4.34	1.6346	$ H - 5 \rightarrow L + 1\rangle + c.c.$ (0.6014) $ H - 4 \rightarrow L\rangle + c.c.$ (0.1293)
$V_{x\&y}$	1B_1	4.55	0.3654	$ H - 2 \rightarrow L + 2\rangle$ (0.8013) $ H - 3 \rightarrow L + 3\rangle$ (0.2901)
	1A_1	4.60	0.9456	$ H - 2 \rightarrow L + 3\rangle + c.c.$ (0.6069) $ H - 3 \rightarrow L + 4\rangle - c.c.$ (0.0666)
$VI_{x\&y}$	1A_1	4.98	0.5727	$ H - 9 \rightarrow L + 1\rangle + c.c.$ (0.5173) $ H - 2 \rightarrow L + 5\rangle + c.c.$ (0.2263)
	1B_1	5.05	0.4499	$ H - 4 \rightarrow L + 2\rangle - c.c.$ (0.5437) $ H - 1 \rightarrow L + 8\rangle - c.c.$ (0.2051)
$VII_{x\&y}$	1B_1	5.62	0.7449	$ H - 2 \rightarrow L + 6\rangle - c.c.$ (0.5213) $ H - 1 \rightarrow L + 10\rangle + c.c.$ (0.2595)
	1A_1	5.65	0.3769	$ H - 10 \rightarrow L\rangle - c.c.$ (0.5275) $ H - 3 \rightarrow L + 6\rangle - c.c.$ (0.2146)
$VIII_y$	1A_1	5.89	0.5315	$ H - 3 \rightarrow L + 8\rangle - c.c.$ (0.4836) $ H - 9 \rightarrow L + 2\rangle + c.c.$ (0.2443)

Table S21: Continued from the previous table: excited states giving rise to peaks in the singlet linear absorption spectrum of GU-42 (C_{2v} symmetry), computed using the MRSDCI approach, and the screened parameters in the PPP model. Subscripts x and y on a peak label, indicate the polarization direction of the absorbed photon.

Peak	Symmetry	Energy (eV)	Transition Dipole (\AA)	Dominant configurations in the many-body wave function
$IX_{x\&y}$	1A_1	6.19	0.3012	$ H - 7 \rightarrow L + 4\rangle - c.c.(0.4635)$ $ H - 5 \rightarrow L + 8\rangle - c.c.(0.2752)$
	1B_1	6.22	0.6616	$ H - 7 \rightarrow L + 5\rangle + c.c.(0.5310)$ $ H - 4 \rightarrow L + 6\rangle + c.c.(0.2804)$
X_y	1A_1	6.60	0.5128	$ H - 3 \rightarrow L + 10\rangle + c.c.(0.5870)$ $ H - 9 \rightarrow L + 4\rangle - c.c.(0.0983)$

Table S22: Excited states giving rise to peaks in the singlet linear absorption spectrum of GU-42 (C_{2v} symmetry), computed using the MRSDCI approach, and the standard parameters in the PPP model. Subscripts x and y on a peak label, indicate the polarization direction of the absorbed photon.

Peak	Symmetry	Energy (eV)	Transition Dipole (\AA)	Dominant configurations in the many-body wave function
I_x	1B_1	3.53	2.560	$ H - 1 \rightarrow L + 1\rangle$ (0.5919) $ H \rightarrow L\rangle$ (0.468)
II_x	1B_1	4.10	1.259	$ H - 2 \rightarrow L + 1\rangle + c.c.$ (0.4275) $ H \rightarrow L + 3\rangle - c.c.$ (0.4041)
III_y	1A_1	4.37	2.702	$ H - 2 \rightarrow L\rangle + c.c.$ (0.4471) $ H - 1 \rightarrow L + 3\rangle - c.c.$ (0.3548)
IV_x	1B_1	4.61	1.171	$ H - 1 \rightarrow L + 1\rangle$ (0.3140) $ H - 3 \rightarrow L\rangle - c.c.$ (0.3071)
V_y	1A_1	4.94	1.264	$ H - 5 \rightarrow L + 1\rangle + c.c.$ (0.3673) $ H - 4 \rightarrow L\rangle - c.c.$ (0.2669)
VI_x	1B_1	5.09	0.9065	$ H - 8 \rightarrow L + 1\rangle - c.c.$ (0.3051) $ H - 5 \rightarrow L + 5\rangle$ (0.2888)
VII_x	1B_1	5.31	1.0260	$ H - 5 \rightarrow L\rangle + c.c.$ (0.3978) $ H - 7 \rightarrow L + 3\rangle + c.c.$ (0.1846)
$VIII_y$	1A_1	5.50	0.9967	$ H - 5 \rightarrow L + 1\rangle + c.c.$ (0.3690) $ H - 7 \rightarrow L + 1\rangle - c.c.$ (0.2591)
$IX_{x\&y}$	1A_1	5.84	0.7460	$ H - 3 \rightarrow L + 2\rangle - c.c.$ (0.2710) $ H - 1 \rightarrow L + 9\rangle - c.c.$ (0.2563)
	1B_1	6.00	0.5885	$ H - 3 \rightarrow L + 3\rangle$ (0.2872) $ H - 3 \rightarrow L + 5\rangle - c.c.$ (0.2691)
$X_{x\&y}$	1A_1	6.22	0.3977	$ H - 1 \rightarrow L + 7\rangle - c.c.$ (0.3639) $ H - 7 \rightarrow L + 2\rangle - c.c.$ (0.2225)
	1B_1	6.42	0.5896	$ H - 1 \rightarrow L + 10\rangle + c.c.$ (0.3326) $ H - 5 \rightarrow L + 5\rangle$ (0.2806)

Table S23: Continued from the previous table: excited states giving rise to peaks in the singlet linear absorption spectrum of GU-42 (C_{2v} symmetry), computed using the MRSDCI approach, and the standard parameters in the PPP model. Subscripts x and y on a peak label, indicate the polarization direction of the absorbed photon.

Peak	Symmetry	Energy (eV)	Transition Dipole (\AA)	Dominant configurations in the many-body wave function
XI_y	1A_1	6.59	0.4713	$ H - 4 \rightarrow L + 5\rangle - c.c.(0.3327)$ $ H - 8 \rightarrow L + 3\rangle + c.c.(0.2854)$
$XII_{x&y}$	1A_1	6.90	0.7306	$ H \rightarrow L + 13\rangle + c.c.(0.2390)$ $ H - 7 \rightarrow L + 2\rangle - c.c.(0.2364)$
	1B_1	7.01	0.2492	$ H - 12 \rightarrow L\rangle - c.c.(0.3780)$ $ H - 1 \rightarrow L + 14\rangle + c.c.(0.2648)$
$XIII_y$	1A_1	7.33	0.5609	$ H - 6 \rightarrow L + 7\rangle - c.c.(0.3383)$ $ H \rightarrow L + 14\rangle + c.c.(0.1862)$
$XIV_{x&y}$	1B_1	7.45	0.6663	$ H - 11 \rightarrow L\rangle + c.c.(0.2983)$ $ H - 8 \rightarrow L + 8\rangle(0.2825)$
	1A_1	7.50	0.3916	$ H - 5 \rightarrow L + 6\rangle + c.c.(0.2588)$ $ H - 7 \rightarrow L + 8\rangle + c.c.(0.2524)$